MODELING THE LUBRICATING INTERFACES OF HIGH PRESSURE RADIAL PISTON MACHINES

A Thesis

Submitted

In Partial Fulfillment of the Requirements

For the Degree of

MASTER OF TECHNOLOGY

In

Production and Industrial Engineering

Submitted by

Ankit Kumar

Under the Supervision of

Mr. Yaqoob Ali Ansari

Assistant Professor

Department of Mechanical Engineering

Faculty of Engineering

INTEGRAL UNIVERSITY,LUCKNOW,INDIA

June,2022

CERTIFICATE

This is to certified that **Mr. Ankit Kumar (Enroll No-1900104132)** has carried out the research work presented in this thesis **" MODELING THE LUBRICATING INTERFACES OF HIGH PRESSURE RADIAL PISTON MACHINES"** submitted for partial fulfillment for the award **Degree of Master of Technology in Production and Industrial Engineering** from **Integral University, Lucknow** under my supervision .Thesis embodies results of original work, and studies are carried out by the student himself and the contents of the thesis do not form the basis for the award of any other degree to the candidate or to anybody else from this or any other University/Institution.

Signature of Supervisor

Full Name: **Mr. Yaqoob Ali Ansari**,

Designation: Assistant Professor,

Department of Mechanical Engineering

Integral University, Lucknow.

Date:

Place:

DECLARATION

I hereby declare that the thesis titled "**MODELING THE LUBRICATING INTERFACES OF HIGH PRESSURE RADIAL PISTON"** is an authentic record of the research work carried out by me under the supervision of Mr. **Yaqoob Ali Ansari Assistant Professor, Department of Mechanical Engineering, Integral University, Lucknow**. No part of this thesis has been presented elsewhere for any other degree or diploma earlier.

I declare that I have faithfully acknowledged and referred to the works of other researchers wherever their published works have been cited in the thesis. I further certifythat I have not willfully taken other's work, text, data, results, tables, figures etc.reported in the journals, books, magazines, reports, dissertations, theses, etc., or available at web-sites without their permission, and have not included those in this Master of Technology thesis citing as my own work.

Date: Signature: _____

Name:**Ankit Kumar**

Enroll.No:**1900104132**

ACKNOWLEDEMENT

I would like to express my deep sense of gratitude, respect and honor to my supervisor **Mr. Yaqoob Ali Ansari, Assistant Professor, Department of Mechanical Engineering, Integral University, Lucknow**, for his illuminative and precious guidance, constant supervision, critical opinion and timely suggestion, constant useful encouragement and technical tips which has always been a source of inspiration during the preparation of dissertation. I consider myself extremely lucky to be able to work under the guidance of such a dynamic personality.

I would also like to thank the rest of dissertation committee, **Prof. Dr Prem Kumar Bharti (HOD) Department of Mechanical Engineering ,** my dissertation **Incharge Dr Mohd. Anas Associate Professor,** Entire Faculties and staff of **Department of Mechanical Engineering** for their supports, encouragement and providing me the opportunities while working on this exciting research.

I will be failing in my duties if I miss to express my profound and deepest sense of gratitude to my beloved parents and other members of family and friends for their keen interest in my studies, immense support and encouragement , without which it was impossible to complete this dissertation.

I also place on record my sense of gratitude to one and all who directly or indirectly. Have lent their hand in this thesis.

Date: Signature: _____

Name: **Ankit Kumar**

Enroll.No:**1900104132**

TABLE OF CONTENTS

LIST OF TABLES

LIST OF FIGURES

ABSTRACT

Radial piston pumps Positive displacing machines, such as radial piston devices, are normally employed in greater hydraulic operations. Their relatively compact structure enables them to withstand very extreme pressure at minimal shaft speeds. , it is critical that they be both highly efficient and long-lasting.

The primary purpose of this study was to use virtual prototyping to help with thedevelopment of effective and long-lasting radial pistons machines. To that purpose, numerical and experimental methodologies were developed to investigate the greasing interfaces in a specific reference device and recommend design adjustments which would allow similar devices to operate more efficiently and in complete film lubricant regime

A unique Integrated Fluid Structural Interactions (FSI) oriented Elastohydrodynamic (EHD) framework for flow via the piston/cylinder contact was presented to accomplish this goal, taking into account various coupled processes like:

1.The lubrication gaps flow pressures and velocity created by the piston/cylinder
2.The piston' micro-motion inside the fixed cylinder
3.The lubrication fluids inside the gap and the elasto-plastically distorted deformationexisting on the surface of solid elements (i.e. pistons and cylinders) share the burden.
4.Elastic distortion of solid material caused by fluid stress in the gaps and impingement contacting stresses in addition to provide methods that result to the lubricating changing from of the mixed-EHD domain to the complete EHD regime.

The findings of this study revealed that numerical modeling of radial piston engines could allow virtual prototype, saving the time, energy, and equipment in comparison to manual development and testing. Thermal impacts in both the lubrication gap can be used in researching the gaps flow as parts of the model's subsequent improvement.

A heterogeneous lubrication approach for the cam/piston contact, as well as the inclusion of squeezing forces, could result in even better piston micro-motion forecasts. Finally, an optimisation process might be devised to assist in the development of most effective and long-lasting groove piston design for diverse radial piston equipment and related

CHAPTER 1
INTRODUCTION

1.1 Overview of Radial Piston Devices

Positive displacement devices, such as radial piston devices, are normally employed in greater hydraulic operations. Radial piston pumps offer higher efficiency than other piston pumps since typically only have two lubrication contacts. Their relatively compact structure enables them to withstand very extreme pressure at minimal shaft speeds. These characteristics make such designs extremely effective in uses like as hydraulic transmission motor, winds power pump units, fixed automated processes like hydraulic pumps, bolt belt tensioner, and rock splitters, and so on. Because of the tremendous demand for these machines in various applications, it is critical that they be both highly efficient and long-lasting.

There appear to be two types of radial piston devices in total: moving cam and rotating cylinder. The pistons in a rotating cam type engine rest on an internal eccentric cam whose revolution controls their motion; in a rotating cylinder type device, the pistons rest on an outside fixed ring while a cylinder body in the center spins. The hypothetical designs for both of these kinds of machines are shown in Figure 1.

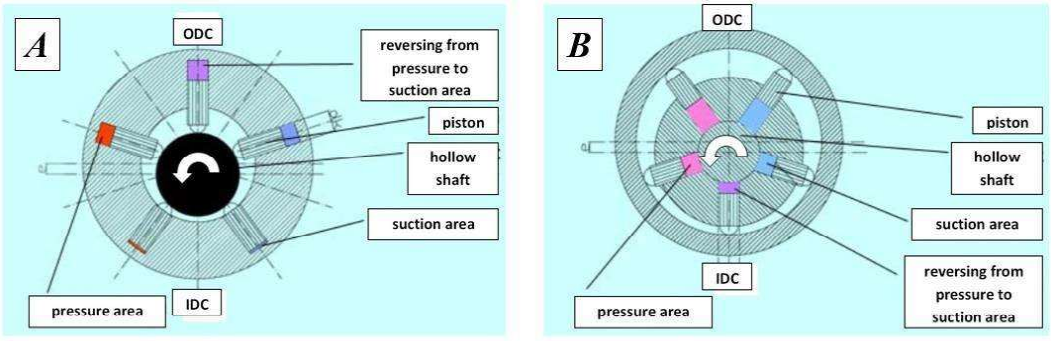

Figure1: Units with rotating cams and cylinders are (A) and (B), respectively.

1.2 Interfaces in Tribology

Figure 2 displays a rotating cam type radial pistons pump component that will be the subject of this investigation.The hydraulic cylinder contact (Figure 3) as well as the cam/piston junction (Figure 4) are the two fundamental tribological contacts in these devices (Figure 4). The load carrying and sealing capabilities of these lubrication gaps are their principal roles. In order to minimize plating wear and, subsequently, unit breakdown, the lubricating coating within those places should be strong enough to carry the extra stress. Moreover, the presence of this load-bearing fluid layer shows that all of these systems are vulnerable to efficiency losses caused by leaks (at the piston/cylinder contact) and viscosity resistance generated by fluid shear (in both interfaces). Designing the piston/cylinder contact to avoid power inefficiencies is a tough undertaking. There are two types of losses: leakage-related and viscoelastic frictional power dissipation.While viscosity shear loss tends to rise with reduced contact gap altitudes, leaking tends to increase with higher lubricating film thickness between piston and cylinder.

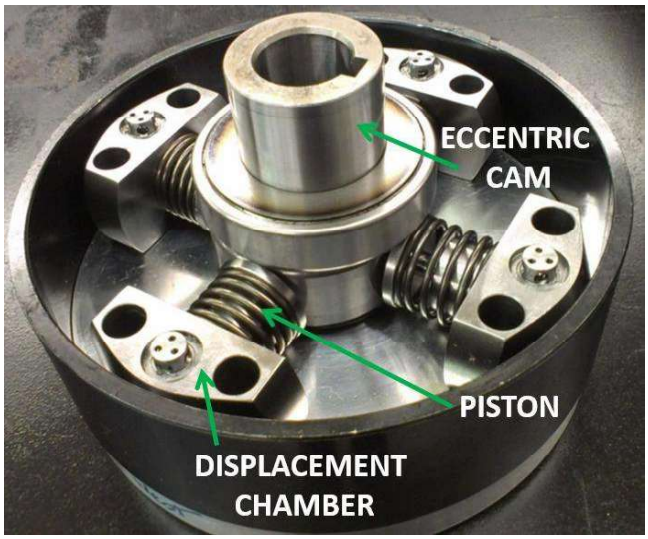

Figure2: Pump unit having radial pistons that rotate on cams.

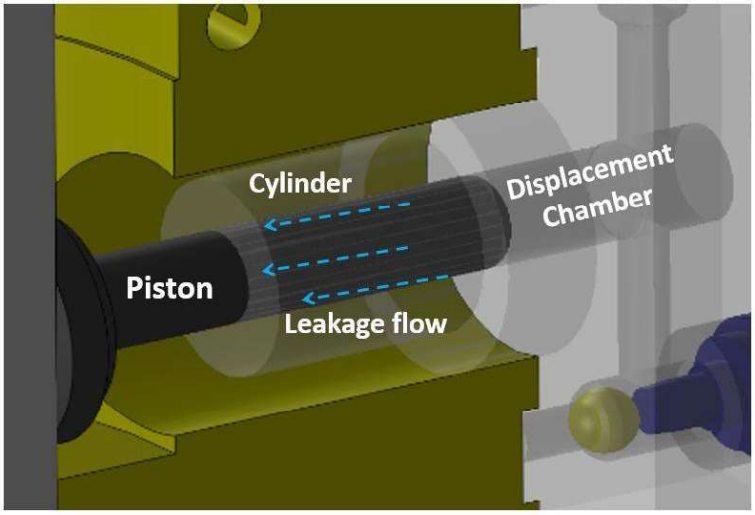

Figure3:An illustration of a radial piston pump's piston/cylinder contact and the leakage it causes.

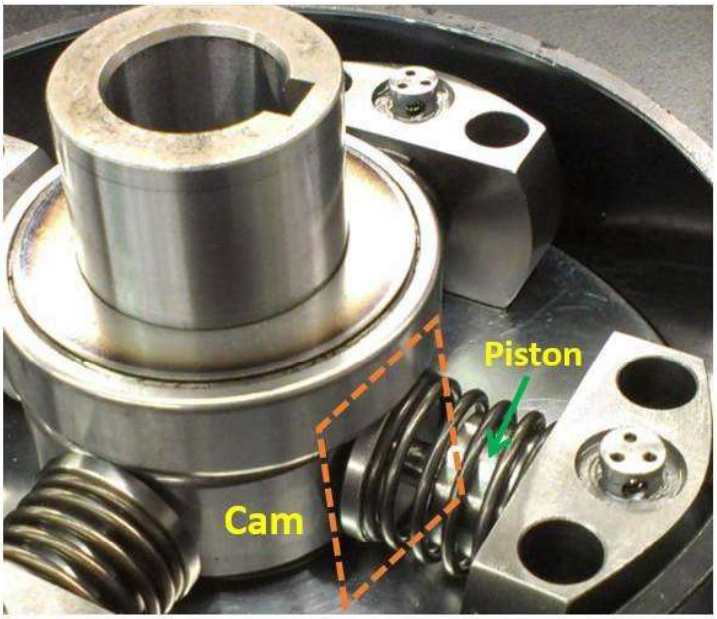

Figure4: The cam/piston contact interface of a typical radial piston pump

The fundamental concern in reducing viscous frictional forces at the cam/piston junction in radially piston devices is ensuring that the gap widths at the cam/piston interface are adequate. However, due to the large, continuously fluctuating pressures acting at the interface and the relatively modest working speeds, this task is easier said than done. As a result, a thorough examination of these interfaces is required in order to construct functional units using virtual prototypes, which is one of the research's objectives.

1.3 Pump Reference Design

Although radially piston devices are capable of serving mostly as a hydraulic pump and a motor, in this study, a rotational cam type pump would be utilized as a reference. The contacts of the standard pump evaluated in this work are shown in Figures 2 and 4. The many elements of the architecture under consideration are illustrated by Figure 5's top image of the pump. The device employed in this investigation has a capacity of 1.0 cc/rev and a maximum operating pressure of 700 bar.

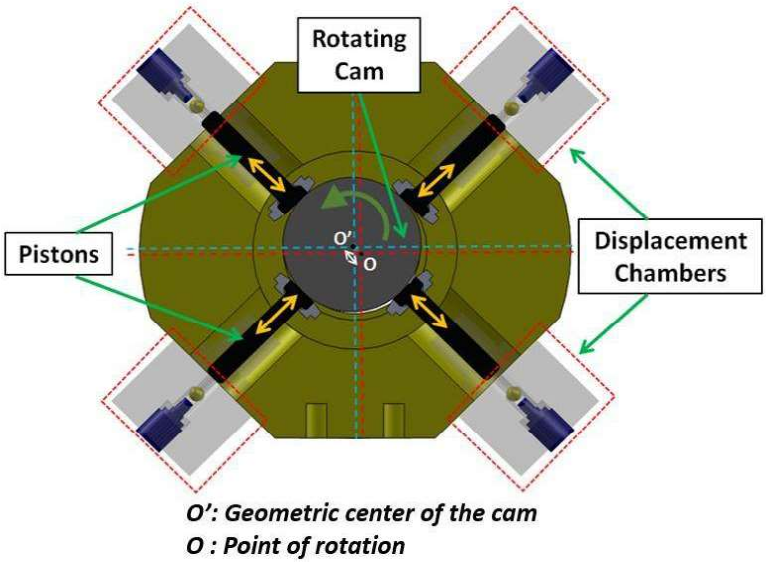

Figure5:View of the reference radial piston pump unit from the top, highlighting its essential elements.

This unit's functioning is simple: the lower pressures (LP) channel collects water from of the suction pipe and transfers it all to the 4 displaced compartments. The pump requires a boost pumping system since the LP channel is pressurized instead of being an open-circuit voltage design that draws fluid from ambient pressure (not shown here). This configuration is described in further detail in [6].The entrance and departure of the liquid inside every displacement chamber is controlled by two pairs of inlet and the outlet spherical control valve. The revolving movement from each of the 4 cylinders inside their corresponding displaced chamber is caused by the movement of an eccentricity cam, which provides the pressure gradient. The liquid is delivered at elevated pressure through high force (HP) path to the pump's distribution port. To maintain the fluid at the right pressure, a pressure regulator is employed. The pneumatic tool that will be controlled has

this distribution module attached.Figure 6 shows how this technique works.

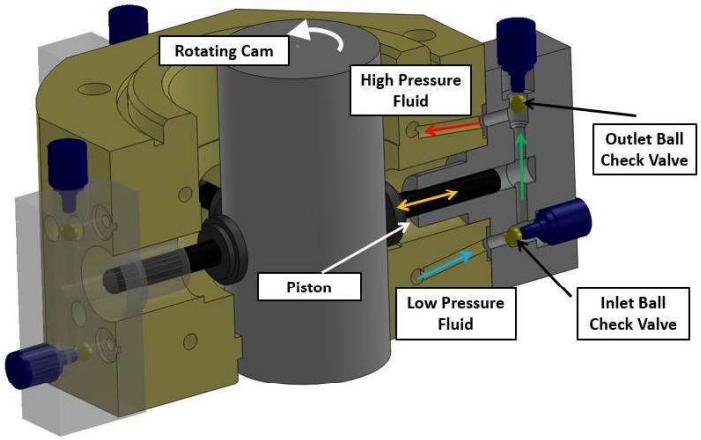

Figure6:A complete view of a displacement chamber demonstrating the operation of a radial piston pump unit.

Because of surfaces shear from higher contact stresses, spinning cam style radial pistons units are inclined to excessive wearing at the cam/piston junction. The eccentric cam is maintained by moving component bearings that sit on a free-to-rotate surface of the shell that would be in touch the with cylinders in order to avoid this (Figure 7).

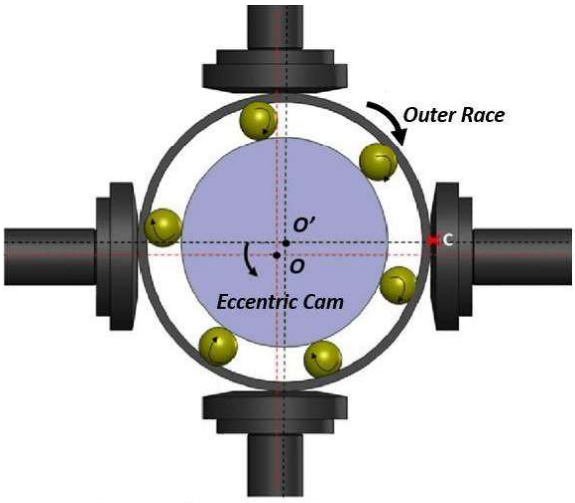

Figure7: The eccentric cam, rolling element bearings, and outer race that sits on each piston of a radial piston pump are illustrated..

1.3 Research Objectives

The primary purpose of this study was to use virtual prototyping to help with the development of effective and long-lasting radial pistons machines. To that purpose, numerical and experimental methodologies were developed to investigate the greasing interfaces in a specific reference device and recommend design adjustments which would allow similar devices to operate more efficiently and in complete film lubricant regime.

A unique Integrated Fluid Structural Interactions (FSI) oriented to overcome this problem, an electrohydrodynamic (EHD) framework for flow via the piston/cylinder contact was described, taking into consideration several coupled processes like as:

• The lubrication gaps flow pressures and velocity created by the piston/cylinder

• The piston' micro-motion inside the fixed cylinder

• The load is split between the lubrication fluids in the gap and the elasto-plastically distorted deformation existing on the face of solid parts (such as piston and cylinders).

• Elastic deformation of solid materials induced by fluid stress in gaps and impingement contacting stresses, as well as ways for lubricating the transition from the mixed-EHD domain to the entire EHD phase.

This combined lubrication system was designed primarily to examine the effect of surface morphological alterations, such as creating circumferential piston notches to improve piston tilt balance inside the cylinders, on proper film lubrication during pump operations. By measuring the inefficiencies in the piston/cylinder lubrication gap, the models were also utilized to examine the impact of these notches in increasing the pump's lubrication efficiency.

The development of an experimental method to study the movement of the completely free outermost races due to dynamic load levels of all four piston during in the pump operating period was another unique addition of this research. The study's findings were paired with a previously published computational approach to quantify the frictional force at the cam-piston interface. This enabled us to estimate the frictional contact acting on the piston as a result of the outer ring altering the vibration of the piston under all flow conditions more precisely.By addressing crucial physical impacts both in lubricating surfaces present, the methodologies proposed in this study offer great potential in the simulated design of effective and useful highly pressurized radial piston engines. This programme can also be used to investigate surface characteristics and examine novel radial pistons machine layouts.

CHAPTER 2.

LITERATURE OVERVIEW

The material relating to the many parts of the current study has been divided into multiple parts in this chapter. Various modelling methodologies used for characterizing the architecture of affirmative motion machineries have been emphasized, with a particular emphasis on modelling lubricating surfaces.

2.1 Radial Piston Machine Modeling

Radial pistons engines are currently developed, on the whole, through a series of tests that are both expensive and time consuming. As a result, minimal work on modelling of these differential pressure devices has been documented. For the study of issues affecting motor function, such as resistance in ball joints, Chapple [1] constructed an analysis method of a rotary piston motor. While the emphasis of this study was on the various loads applied to the components and the movement provisions associated with them, the flow characteristics of the motors were not explored. Ivantysyn and Ivantysynova [2] created kinematic relationships and pressure assessments to characterize the flows in radial piston engines with rotating cams and revolving pistons. Kleist [3, 4] devised an isothermal model to characterize the gaps flowing in radial piston engines. This assumption, however, was based on the assumption that the moveable portions behaved like rigid bodies. Mortenson [5] examined the efficiency of a wind transmitting system's circular piston pump.Whereas the flow characteristics were explored in depth, the lubricating gap were modelled using a simple assumption.

Agarwal et al. (2014) [51, 52] created a multi-simulation platform to explore the flow characteristics of a radially piston pump, which they then combined with the FSI- EHD models to analyze the piston/cylinder lubrication interaction. To the best of the researchers' knowledge, Agarwal (2014) investigated resistance at the cam/piston intersection in radially piston engines [6].This research builds on the prior work [6].

2.2 EHD models for tribological interfaces

The examination of lubrication surfaces in differential pressure motors has been a focus of study in recent years. Several studies emphasize the need of evaluating the effect of

micro-motion on the mobile components that comprise these interactions. Fang and Shirakashi (1995) were the first to develop a method for anticipating piston position in axial-flow engines that relied on force balance and contact pressure in the piston/cylinder contact [7]. Olems (2002) improved on this research by employing a non-isothermal framework [8].CASPAR, a modeling tool which analyses the three lubrication gaps available in a swash plate kind axial piston engine [9], was developed by Wieczorek (2002) using Olem's methodology. This phenomenon was also used to study the tilting of the gear and lateral plate in the horizontal lubrication interface of exterior gear machineries (EGMs) [10].

Piston / Cylinder Interface [9, 11-16], Shoe / Slanted Plate Interface [17, 18], and Cylinder Block / Valve Plate Interface [19-21], Detailed Model of the Thermal and Elastic Interfaces The one with the metamorphosis effect was created. The EGM performed a similar assessment [10, 22] of horizontal lubrication contact between the gear and the horizontal plate.Each of these simulations shows good agreement with the experimental data, emphasizing the need to add EHD and thermal effects to the differential pressure device.

In addition to positive displacement machines, acceptable contacts include journal bearings [23-26], connecting rod bearings [27], and non-meshing spur gears [28].

2.3 Mixed Elastic Fluid Lubrication

The mean Reynolds method equation [29] established by Patir and Cheng is commonly used to estimate the lubrication current of the non-uniform lubrication regime (1978). When the flow through a coarse bearing is compared to the flow via a smooth bearing, pressure fluctuation is eliminated. To make use of the flow Chengwei and Linqing (1989) proposed a typical expression for Gaussian dispersion on the surface using the Reynolds equation [32]. Lee and Ren (1996) created a complete asperity touch model by incorporating elastic strains of surface asperity [30]. To explain the interaction of surface properties with flow, Harp and Salant (2000) introduced an inter-asperity vortex sub model [33]. Mengetal. (2010) Proposed to consider touch components when modeling the Reynolds flow equation for each continuous measurement [31]. Modelling mixed lubricating in transdermal contact has progressed significantly. For first time, Shi and Wang (1998) published a mixed-the-thermo-electrohydrodynamic (TEHD) models for the lubrication surfaces in journals bearing [34]. The stress assistance due to deformation, on the other hand, was assessed utilizing simplified methods.

Wang et al. (2002) refined the contact impingement interaction in the previous works by incorporating elastic-plastic deflections of the interface asperities [23, 35]. Kraker et al. (2007) used a hybrid method with a modified security interaction model [36] to produce Stribeck curves for water-lubricated journal bearings.There have been a few notable breakthroughs in the subject of mixed lubrication modelling in the realm of hydraulics. Yamaguchi and Matsuoka (1992) presented a combined lubrication model for hydraulic machinery bearing & seal parts [37].

Kazama and Yamaguchi (1993) employed a mixed lubrication technique in hydraulic machinery thrust bearings [38]. Kazama (2005) [39] developed a quantitative simulation framework for the slipper in a blended water hydraulic pump and motor. Fang and Shirakashi (1995) looked at the combined lubrication characteristics of the pistons and cylinders [7] in an axially piston swash plates type piston pump-motor. Wegner et al. (2016) verified an empirical approach for the cylinder block/valve plates interface of axial piston machines [40], which included the impacts of surface quality, solid contact, surface displacement, and micro-motion.

2.4 Surface Modification Effects on Lubrication Performance

Micro-surface form in axial piston devices has been a study focus for many years. Various piston surface characteristics such as the barrel form, a sine waved barrel, a half barrel shape, and a sine wave have all been widely investigated [41, 42]. Ivantysynova and Garrett (2009) have even applied for patents for a sine wave form piston, which has a maximum power loss reduction of 60% in simulation [43]. Even though the type of alteration explored in this study is a groove, which falls under the category of surface treatments with scale lengths on the order of mm, it is crucial to emphasize that micro-surface shaping offers similar benefits.

Many studies on grooves insertion have been conducted. In oil-lubricated axial-flow machines, Park (2008) [44] looked at the effect of the cylinder groove on pressure build-up at the piston/cylinder contact. Berthold (1999) submitted an invention for using pressured circular grooves in axial - flow machines' cylinder bores, in which the groove is linked to the unit's highly pressurized side and help to cylinder balance the piston [45].
Majumdar et al. (2004) examined the effects of altering the axis. groove width in water-lubricated journals bearing on the stability of the journal as well as the interface's significant performance [46].Basu (1992) replicated radially grooved face seals using a computer simulation [47]. Razzaque et al. (1999) [48]

CHAPTER 3

USING NUMERICAL MODEL ANALYSIS OF LUBRICATION PERFORMANCE

3.1 Simulation Software for Multi-Domain

This chapter discusses simulation software for multi-domain developed by the Maha Fluid Power Center [51, 52].This tool contains a number of modules needed to study the lubrication effect of radial piston pump systems with camshafts. Figure 8 shows the general architecture of simulation software, including the many sub-models generated, and the interaction of the data between each of these sub-models.

Flow variables such as cam or piston movement, flow and pressure ripple in the exhaust pipe, momentary pressure difference in one of the dispersion chambers, and flow of two existing lubrication joints (piston / cylinder interface and cam). Characteristic modeling / piston interaction-one of the features of the simulation software.

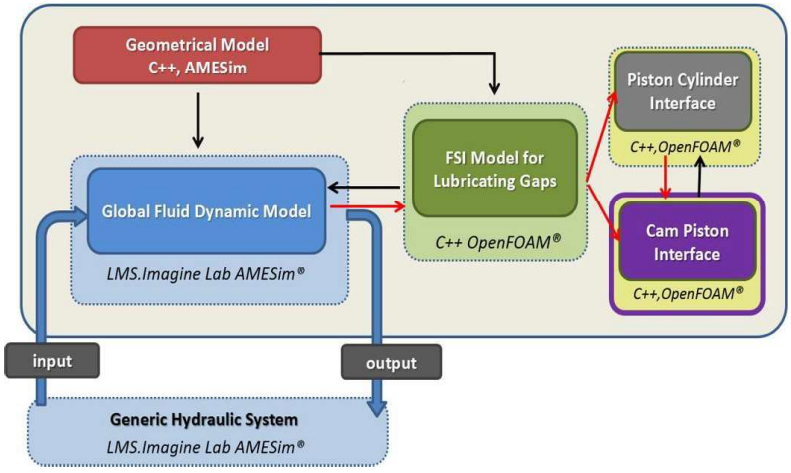

Figure8:The graphical representation of simulation tool for radial piston machines.

Each of the components utilized to investigate the many variables necessary to describe a radial piston pump is briefly discussed in the following chapters.

3.1.1 Geometric Model

The geometrical modeling is in charge of calculating the cam's and each piston's kinematic parameters. The data produced here are fed into the other module that analyses the pump's flow characteristics. This simulation is a standalone program written in C++ that can calculate kinematic characteristics for cam and piston surface of any shape. The following are the numerous parameters that were analyzed for use in different modules:

*Model of Global Fluid Dynamics: Model of Global Fluid Dynamics:*For this purpose, immediate values of piston displacing, dispersion chamber sizes, and translating piston velocity are produced.

Piston/Cylinder Gap Model: The contacting pressure there at cam/piston interaction operates at this point, generating film between the piston cylinder for the lubricating oil in its immediate duration and establishing the coordinates of the point of contact in the pistons and cams.

Cam/Piston Gap Model: The interface velocity variables in the EHL line interaction model are calculated using Cam/Piston contacting parameters.

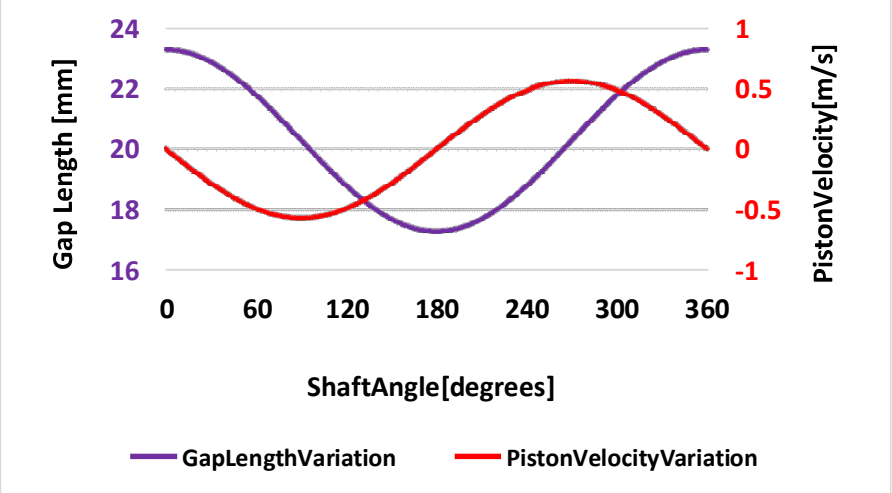

Figure9:During a single pumping cycle, the cylinder and piston gap length

Figure 9 . The graphs depict the instantaneous measurements of each variable during a shaft revolution depicts a few of the key geometrical characteristics that this model analyses, as well as their variations as a function of shaft angle. A 0o shaft angle corresponds to piston 1 at bottom dead Centre in this case (BDC).

3.1.2 Model of Global Fluid Dynamics

The pressures boundary requirements for the piston/cylinder lubrication gap model are determined using the global fluid flow model in combination with the piston/cylinder lubrication gap model. The purpose of this idea is to illustrate the flow of the full radially piston pumping system. This is accomplished through the use of a lumped variable modelling technique.Other differential pressure machines, such axial piston engines and EGMs, have already successfully employed this method [9, 53], and it has also been confirmed to be used in radial piston computers [51]. The module's main output is an assessment of the essential flow properties in pumping, namely the flow velocity, pressures at the outlet pipe, and pressures within each displaced chamber.

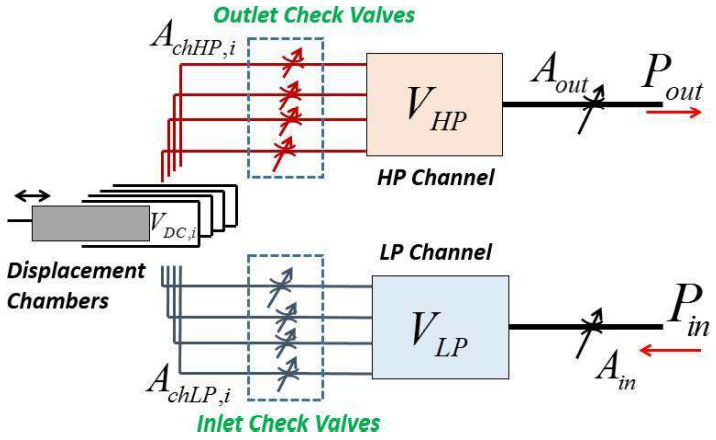

Figure10:The lumped parameter model for the reference radial piston pump is shown schematically.

LMS was used to develop a hydrodynamic model. Consider a LabAMESim® environment that combines a user-defined library with a standard C language library. Each displaced chamber and LP / HP channel is split into different control volumes for the rotary engine. Figure 10 shows the batch variable modeling method used to study the reference model of a radial piston pump. The flow equation is calculated at each control volume and then linked to give different flow variables across the circulator. Figure 11 shows the formulas for a displacement reaction chamber constant volume. The HP and LP channels have similar equations to solve.

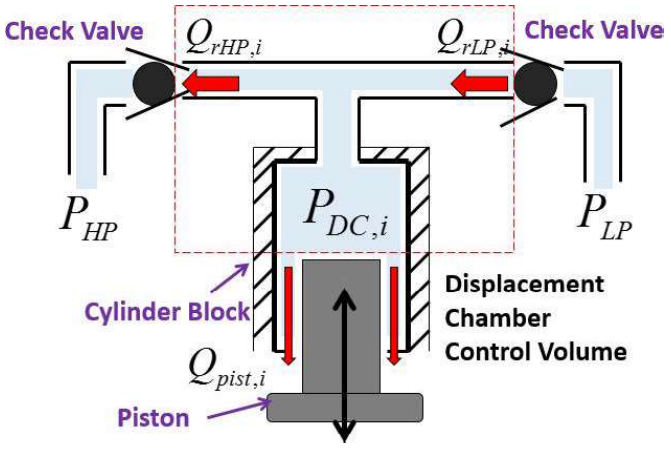

Figure11:Diagram of a single displacement chamber control volume

To forecast the rate of change of pressure in each displacement chamber control volume, the pressure build-up equation is employed

The graphs depict the instantaneous measurements of each variable during a shaft revolution In order to solve the pressure distribution the flow term of each check valve ($QrHP$, i, $QrLP$, i) near the replacement chamber is required. These are obtained by solving the turbulent orifice flow equation.

$AHPv$shows the area of orifice between the HP duct and the exhaust chamber. The opening of the outflow ball check valve determines this (see Figure 11).Similarly, $ALPv$indicates the opening area of the intake ball check valve A thorough selection of AMESim libraries that incorporate the impacts of geometry in detail was used to analyze the valve opening regions in orifice flow equations.

The volume change caused by ball movement in the check valve is taken into account in Equation 3.2 and is incorporated into the valve models. Model the leak through each displacement chamber using a fully defined laminar flow equation that represents the relative motion between surfaces ($Qpist$,):

[51] provides further details on the global hydrodynamic model and its outcomes. Important aspects such as piston vibrations and hydrodynamic effects are not taken into account by the hydrodynamic model. These physical factors have a substantial impact on the computed leak's accuracy. This has an impact on the accuracy of shear and volume losses, which characterize the unit's life. is only used as an initial estimate of leakage to calculate displacement chamber pressure (see Figure 12) and as a boundary condition for a more complicated lubrication gap model that takes into account the aforementioned

impacts. The leaks determined by the gap model are then utilized to control the pressure in the displacement chamber, resulting in the formation of a coupling system. The next part discusses the lubrication gap model for the two interfaces (piston / cylinder interface and cam / piston interface) in the reference design under discussion.

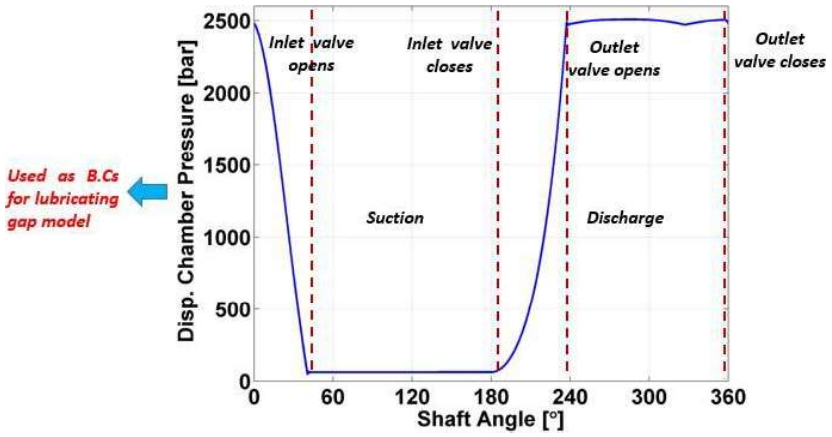

Figure12:Variation in momentary pressure inside a displacement reaction chamber, as well as valve timings, were used as boundary conditions for the gap model.

3.2 Piston/Cylinder Fluid Structure Interaction Model

The FSI model of piston-cylinder contact established in [6, 52] is one of the main components for investigating this lubrication gap in radial piston machines. According to the key assumptions used in the design of this gap model, the load is fully sustained by the fluid membrane between each piston and cylinder throughout the pump operation under all operating conditions. This section describes the FSI piston-cylinder interaction model. This model was developed with numerous physical phenomena that occur in radial piston pumps in mind, like as: B. The liquid film is crushed by the structural elastic deformation of the solid surface (piston and cylinder) due to the high pressure generated in the gap and the fine movement of the piston due to the various forces acting on it. The various sub-models contained in this tool and the flow of information between them characterize these effects. Preprocessors and solvers are two large groups in which sub-models are categorized. The following is an overview of the preprocessor.

Dynamic Fluid Mesh Generator / Solid Mesh Generation: Liquid film architecture (because the piston moves dynamically in the cylinder during the rotation of each shaft) and solid elements mesh within a restricted volume (piston and cylinder)increase. Boundary condition setting: Pressure boundary condition on the fluid network's surface.

The following FSI models are listed.

Gap flow model: Fluid Reynolds technique finite volume solver.

Structural model: Finite volume solution for solid elastic equations, such as those involving pistons and cylinders. Force balance model: Considers the balance of forces operating on the piston

The FSI model is developed as a standalone application utilizing the C ++ programming language, Open FOAM [54] for FV distribution of PDEs associated with linear system solutions, and GSL for multidimensional root-finding techniques and interpolation. It refers to an open-source library like [55].Before delving into the numerous sub-models stated, it is necessary to examine the change in fluid film shape as well as the control variables that drive the simulation.

Piston/Cylinder Fluid Film Geometry

The piston/cylinder geometry is considered to represent axial movement of the piston within the stationary cylinder (sleeve). The varied eccentric motion of the piston with reference to the cylinder axis allows the gap film to squeeze, resulting in a dynamic gap height profile at each position of the piston.

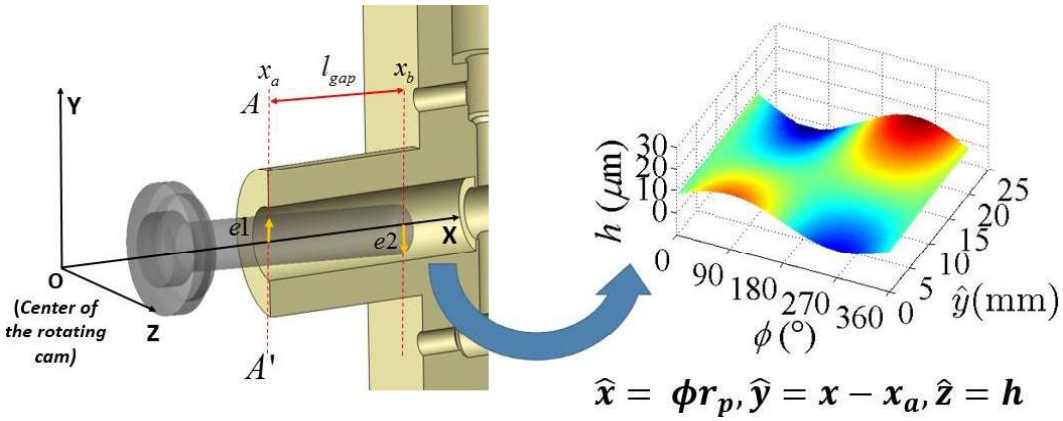

Figure13:Piston tilt settings and arrangement of unwrapped film thickness

Figure 13 depicts the primary geometric parameters that contribute to the distinctive geometry of the piston-cylinder contact. The exact value of the piston eccentricity vector e 1, 2 defined in [6, 52] at each place in the liquid zone determines the local film thickness h. The forces operating on the piston in the current pump design (described in more depth later) are all in the x-y plane (defined in Figure 13), therefore the force acting on the piston along the z-axis is It doesn't cost. When tremors are taken into account, e1

and e2 are adequate to indicate the location of the piston in any configuration.

The piston and cylinder are assumed to be stiff in Equation (3.6). In a genuine pump, the fluid diaphragm is round, but the clearance between the piston and the cylinder is so small in comparison to the piston's diameter that the curvature of the diaphragm form is ignored and fluid pressure production is resolved. To unwrap the film form and show it as a periodic static profile of length 2 rp, you may thus use a Cartesian coordinate system. The enlarged Cartesian coordinate system has the following coordinates:

3.2.1 Boundary Conditions and Mesh Generation

Dynamic Fluid Mesh Generation

A mesh creation module in C ++ was built as part of the FSI model preprocessing to build a mesh for the fluid area. As we saw in the previous section, the unwrapped configuration of the fluid film shows that the calculated fluid region becomes a rectangular Cartesian grid and the height of the gap changes in both $\hat{x}$ and $\hat{y}$ coordinates. Because the lubrication gap domain is defined by micron-order film thickness, changes in fluid pressure in the direction are insignificant, and pressure is only addressed as a function with Figure 14 is an example of a computational grid used for this problem. Because the length of the gap varies with each shaft rotation, a dynamic grating generator is employed to create a grating for each time step over one shaft revolution.

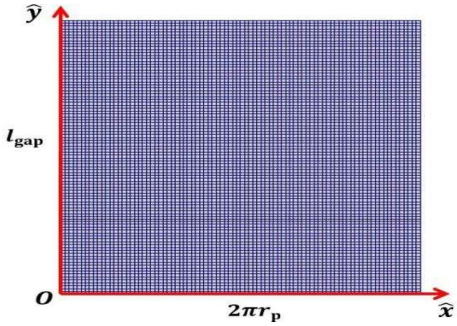

Figure14:The fluid domain in the gap is represented by a conventional computational grid in an unwrapped configuration.

Figure15:(A) Pressure boundary conditions specified at all grid borders, (B) Pressure boundary conditions provided to include boundary pressures at a groove position.

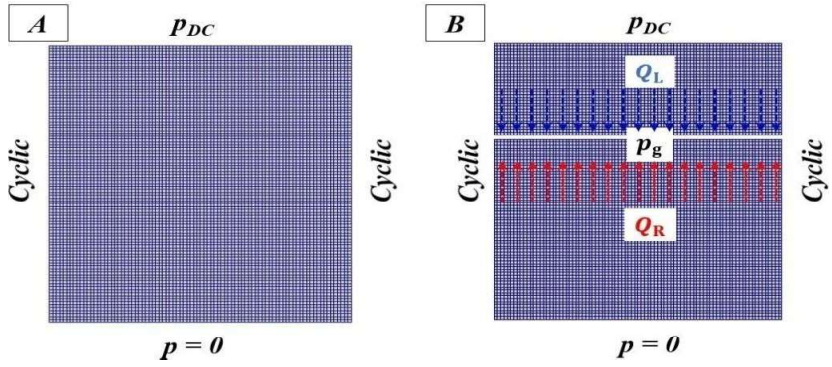

Figure 15 also depicts the boundary conditions that were utilized to solve the pressure in grid computationally (A). The amount of chamber force displaced during shaft rotation is proportional to the engagement limit set on the displaced end of the chamber.

Using the dynamic change in displacement chamber pressure with shaft rotation as computed by a global hydrodynamic model, the instantaneous displacement chamber pressure at each grid produced for one rotation of the shaft is stated(See Figure 12). At the lower limit of the tissue exposed to drainage, the pressure is adjusted to a constant ambient pressure (0 bar). Circular constraints are imposed on the left and right boundaries of the grid. This is because both reflect a collection of the same points in the actual wrapped array. It can be seen that the grid shown in Figure 15 (A) is sufficient to analyze the gap characteristics when the piston does not show exceptional surface features. However, the assumption that a 2D grid may be employed for this analysis fails if the circumferential groove is carved over the length of each piston. Because the gap play is on the order of mm at the groove position, it cannot be considered minor in comparison to the piston's length and circumference. As a result, the control volume technique employed in the lumped constant model is applied to predict the fluid pressure at each groove point.

A 2D mesh can be used to alleviate pressure in the gap everywhere except the groove site for grooved pistons.Because of this, the computational mesh may be separated into several sections, as illustrated in Figure 15. (B). The presence of a groove is shown by the position of each split. The same boundary conditions as in Figure 15 (A) apply here. The presence of the groove, on the other hand, establishes a new border. As a result, in order to measure the pressure at all other places on the grid, the pressure in the groove must be determined. As a result, the pressure increase equation is utilized to calculate groove pressure. This pressure can be used as a boundary condition at the new "groove" boundary on the calculation grid.The equation solved is shown as follows:

3.2.2 Solid Mesh Generation

The solid (piston and cylinder) 3D FV mesh (see Figure 16) was generated using the commercial code ANSYS [56]. For bulk components, a tetrahedral unstructured mesh was chosen because it can be closely matched to the actual geometry.

One of the important features of the FSI model is the dynamic connectivity between the solid and fluid domains, which calls for data to be transferred from the two solid meshes to the fluid meshes and vice versa. To accomplish this, the number of liquid cells was kept substantially larger than the number of fixed meshes, and the closest neighbor

search technique was employed to correlate each solid surface with a group of liquid cells. The next section describes the evaluation of the hydraulic pressure in the cleavage region and the evaluation of structural deformation due to this pressure generation.

3.2.3 Gap Flow Model

The pressure distribution within the piston/cylinder contact is solved using the Reynolds technique, which is derived from the well-known Navier-Stokes equation and takes into account the case's special simplified assumptions. Masu [57]. To account for the predicted deformation of both the piston and cylinder surfaces, a matching form of the Reynolds equation was constructed for the geometry of the radial piston engine's piston / cylinder interface. [6] has a comprehensive derivation of this variant of the Reynolds formula.The dependence of fluid properties contained in Equation (3.10), namely density and viscosity, is modeled using the relationship in [2]. A C++ software that was built was used to implement the Reynolds program's finite volume solver. The pressure is resolved using the conjugate gradient technique, which has been preprocessed with diagonalized incomplete Cholesky [54]. In this investigation, isothermal conditions are assumed. In an early investigation of the lubrication gap [11], it was discovered that the heat influence at the piston-cylinder interface of a piston engine was less significant than the effect of elastic deformation on the total outcome. Because it was discovered in [11] that these impacts were insignificant, we chose not to apply them at this time.However, it will be subject to future investigations and can improve the current FSI model, including the effects of heat generation and thermal deformation.

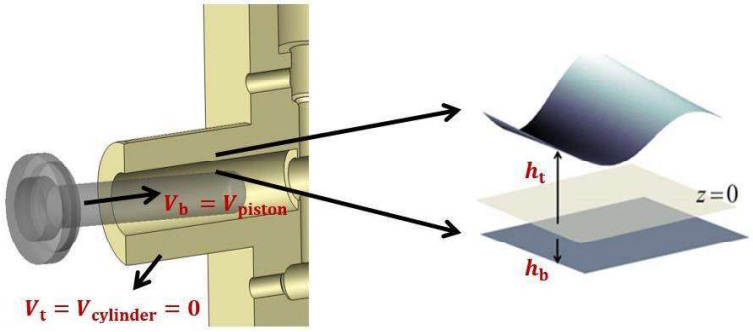

Figure17:The following terms appear in Equation (3.10): top surface (ht) and bottom surface (hb) from a reference plane; stationary cylinder (Vt = 0) and moving piston (Vb = Vpiston).

3.2.4 Structural Deformation Model

The lubrication interface's structural components, notably pistons and cylinders, are subjected to significant compressive stresses and tend to flex elastically. The steady-state finite volume stress / strain formulation proposed in [58] is utilized to simulate solid deformation, which has previously been used to model EGM [10, 22] and radial piston machines [6, 52].

[6] contains a full overview of the many factors that guided the creation and formulation of this FV strain solver. We developed a material deformation matrix for all fixed cells, both pistons and cylinders, using an offline technique known as the influence approach. This is the reference load that is applied to each limit cell. After evaluating the influence matrix (IM), the real compression load fixed limit deformation may be computed utilizing: Δh is the array storing the elastic deflection of each of the solid domain's surface nodes, and pj denotes the external fluid pressure loading on each of the N face of the loaded surface. The influence coefficient IMj indicates the elastic deformation on all surface nodes caused by a reference pressure load preference operating on the jth face. The influence matrix IMDC contains the elastic deformation of all surface nodes caused by the displacement pressure load on the subjected surfaces.

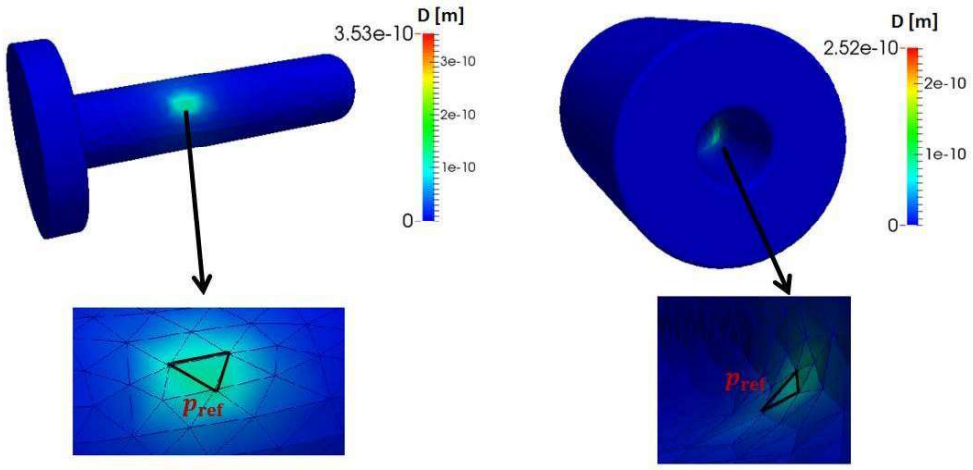

Figure18:Deformationson the surfaces of the piston and cylinder due to a unit pressure applied at a single node. Ideal support constraint has been used for both geometries.

Figure 18 depicts the deformation field of a cylinder and piston when a single cell is subjected to a reference pressure. Ideal support restrictions, including restricting the axes of both geometries, have been introduced. For further detail on the structural model, see [6].

3.2.5 The piston's dynamic load balancing.

The fluid's hydrodynamic pressure operates on the piston at each instant of shaft rotation to properly anticipate the thickness of the lubrication gap. It appears that balance is required. The radial piston machine's fixed operation can balance all external forces. During pump operation, important assumptions include continual film lubrication and no metal-to-metal contact. Figure 19 depicts numerous external influences.

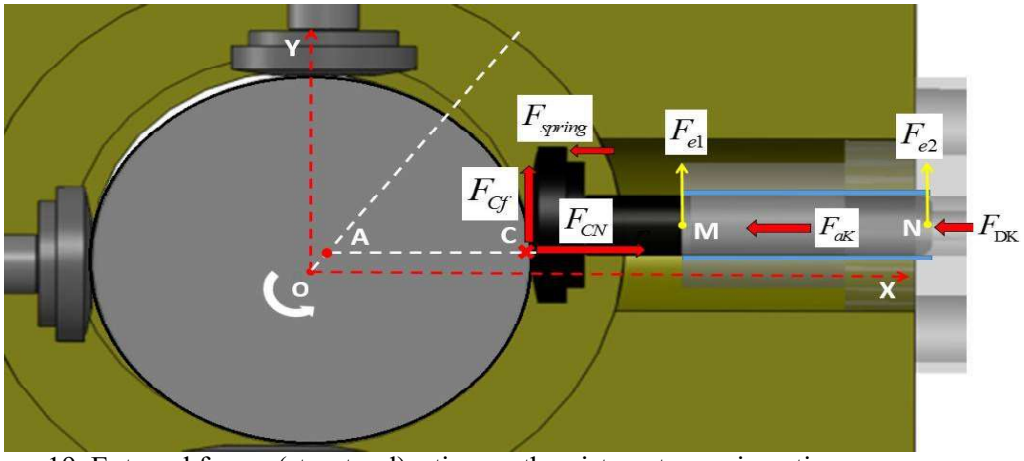

Figure19: External forces (structural)acting on the piston at any given time.

The pressure from the exhaust chamber pressure side FDK exerts the most force on the piston. When these forces diminish throughout the suction stroke, the spring force F spring keeps the piston in contact with the shaft. The spring is present in the reference pump depicted in Chapter 1, although it is not included in the illustration. Because the inertial force operating on the piston was discovered to be minor in comparison to the compressive force of the displacement chamber, it was excluded from this investigation .Another key force is viscous friction, which is created by shearing of the liquid film in the lubrication gap FTf. These forces are balanced along the x axis by the cam response force FCN.

The only lateral load present in the direction y is the frictional force exerted by the cam on the piston. It is based on an offline study of the cam / piston interaction, which is covered in depth in the next chapter. The normal force imparted by the liquid film on the piston surface FTN balances this lateral force. However, because the contact point between the piston and the cam varies with each shaft revolution, the moment is produced by the frictional force FCf and the normal force FCN from the cam. To simplify the calculation process, all external forces and moments acting on the piston are decomposed into an equivalent set of two forces acting on both ends $Fe1$ and $Fe2$. The gap as shown in Figure 19. The value of $Fe1Fe2$ can be obtained by solving the equation

(3.15) – (3.17). In order for the piston to maintain static equilibrium, the external forces and moments acting on the piston must balance the fluid pressure generated in the gap region. A similar process is applied to break down the net effect of fluid force into two forces $Fs1$ $Fs2$ (shown in Figure 20). This is done by equalizing the forces acting in the y direction and balancing the moments around point A.

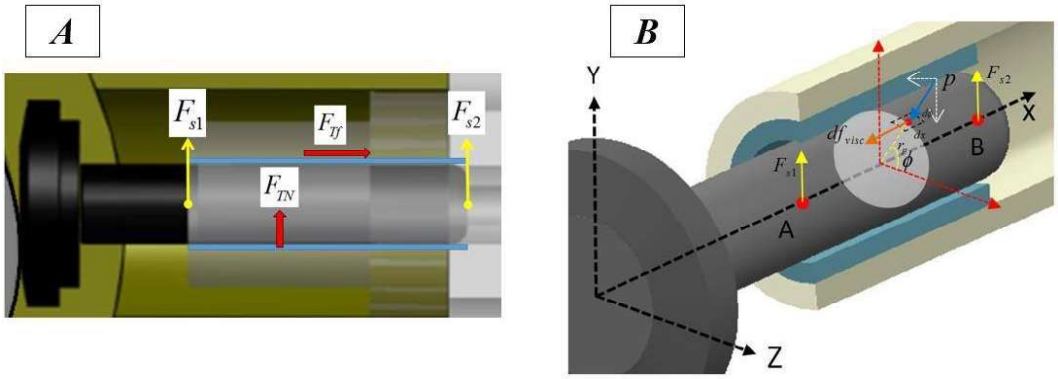

Figure 20: (A) Fluid forces operating on the piston resolved; (B) Resolution of viscous friction forces and response force normal to the piston surface all around its circumference throughout the gap length.

To maintain the computational procedure's stability, when the gap heights fall below a minimum point (hmin = 0.2 m), a virtual contact pressure pc is applied to ensure that the fluid can sustain the stresses occurring at these minimal fluid film sites. The occurrence of this contact pressure under steady-state equilibrium circumstances indicates the presence of a mixed lubrication regime at some places in the piston/cylinder interface During pump operation. The elastic strain is used to evaluate this contact load.

When the gap heights fall below h, the virtual contact pressure pc is used to mimic the impact of a potential solid contact between the piston and cylinder surface. Contact pressure is calculated as:

3.2.6 Coupled Fluid Structure Interaction - Force Balance Solution Algorithm

Figure 21 displays the numerical approach used for the piston/cylinder interaction FSI model. Starting with an initial estimation for the piston eccentricity (tilt), the fluid pressure in the gap domain is computed using the Reynolds equation and utilised to determine deformation in the piston and cylinder faces. This deformation changes the gap's film thicknesses, and the cycle continues until the gap's pressure distribution converges.The force balance condition of the piston is evaluated until equilibrium is reached. Following that, the piston's squeeze velocities are combined to provide the new instantaneous gap film thickness data. This process is repeated throughout the mesh at varied time steps until an overall convergence in film thickness is seen. Figure provides more details on the FSI approach for the interaction between the piston and the cylinder

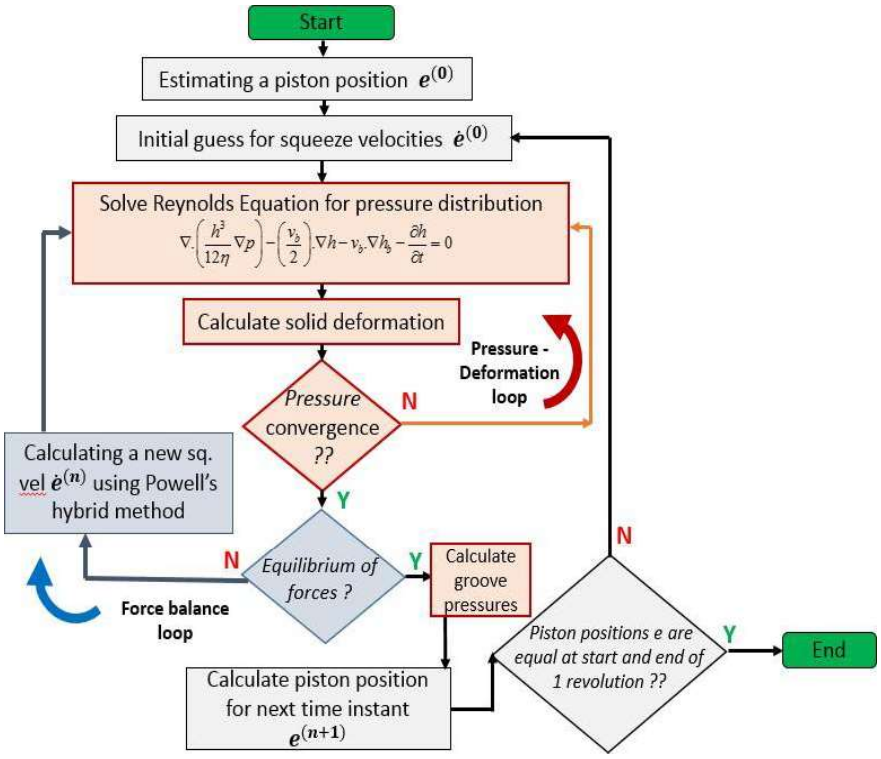

Figure21:Implemented numerical technique for the piston/cylinder FSI-EHD complete film model.

3.2.7 Reasons for Investigating Mixed Lubrication at the Piston/Cylinder Interface

The reference pump piston / cylinder lubrication contact under consideration in this work has previously been studied [6, 52]. The essential assumption in the construction of the FSI model, as previously stated, is that the load during pump operation is totally borne by the liquid film present in the space between the piston and the cylinder. The notional average clearance between the piston and the cylinder is 8 m, according to the CAD drawing of the reference pump under examination.The balancing of the piston forces demonstrates that the cam response force is likewise of this scale because of the extremely high pressure (700–2500 bar) created in the exhaust chamber. Because the point of action of this response force changes as the shaft rotates, a significant moment is created in the piston, causing fine movement. The lateral force (friction) operating between the cam and each piston exacerbates this (Figure 19).The liquid film is therefore anticipated to break in the region of very thin film thickness (2 m). A small movement of the piston might cause this (Figure 22). The lubricant cannot fully sustain the load in the y direction in such locations, and the load is shared by the liquid film and surface.

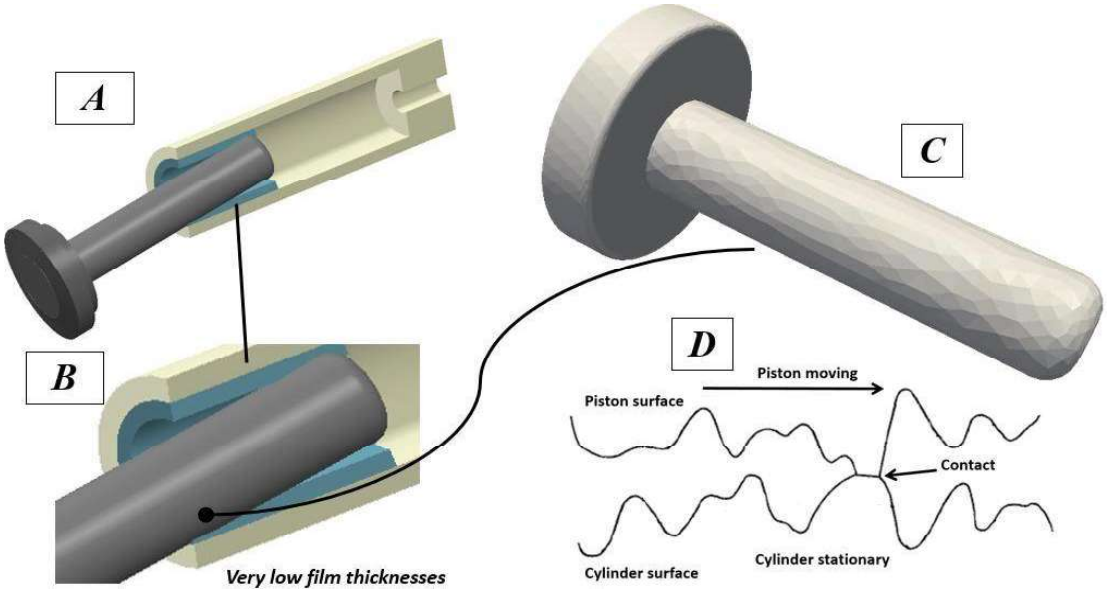

Figure 22: (A) Piston tilting causes a (zoomed in) zone of possible contact in which (C) surface roughness features become crucial to consider, as shown in (D) where there is asperity contact when the gap heights are of the roughness order.

Another reason to investigate blended lubrication at this contact is the effect that circumferential piston groove position has on piston tilt and load balance. In Chapter 6, we will go over the aspect of mixed lubrication in greater detail, as well as an assessment of the pump's lubricating performance. The next part describes the novel Mixed FSI-EHD

(Fluid Structure Interaction - Electrohydrodynamic) model, which was developed to examine the effects of surface roughness and mixed lubrication in radial piston machines.

3.3 Model of the Mixed FSI-EHD Piston/Cylinder Interface

In addition to the sub-models described in Section 3.2, a few more characteristics must be incorporated in order to assess the effect of mixed lubrication in the piston/cylinder gap. The solvers used in this model are briefly detailed below:

Solver for fluid flow: Solves the Reynolds equation for the average flow rate after fluid pressure.

Solver for elastic deformation: Solves a solid's elastic equation. H. Pistons and cylinders control the elastic deformation of the surface caused by fluid pressure building in the gap. This stays unchanged and will not be explored further in the next section. Asperity Contact Solver: Resolves the load borne by elastoplastic ally deformed surface imperfections in thin film thickness areas.

Force balance solver: Balances the force and moment acting on the piston, taking into account the force from bump contact. The information exchange between these solvers and them is highlighted in Figure 23. The various sub-models developed to accurately model the effects of mixed lubrication are discussed in detail in the next section.

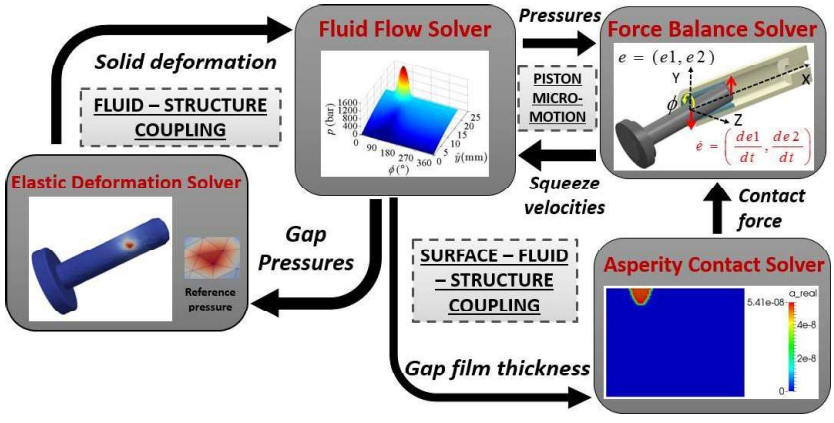

Figure23:The Mixed FSI-EHD solution for the piston/cylinder interaction is depicted schematically.

3.3.1 Assumptions for Considering Surface Roughness Effects

• Several methods exist for simulating the effect of mixed lubrication on lubricated machine components. The most notable feature in the vast literature on this subject is addressing the impact of surface roughness in mixed lubrication models. A stochastic modelling technique is assumed for the objectives of generalizing the surface roughness on the piston and cylinder surfaces. There are several benefits to using this sort of modelling approach, which are mentioned below:

• It provides a statistical representation of surface attributes (such as roughness) for the piston and cylinder, which may be used to newer simulation-based designs that do not require actual measurements.

• Using this approach, you may maintain the assumption you made during unwrapping the 3D gap film to be analyzed as a 2D mesh.

• It is a straightforward approach that can be easily included into the present FSI gap model for the piston-cylinder contact.

• It's been utilized successfully in conformal contact interfaces before [23, 34, 35]. The following presumptions are made before moving on to the specifics of the sub-models when using this approach to model the surface characteristics.:

The heights of the surface asperities are assumed to have a Gaussian distribution. This is an important concern since most surface finishing techniques result in Gaussian distributions (59).

• The surface's qualities are same in both directions of the plane because it is isotropic in nature.

• A surface roughness metric that is coupled Surfaces are characterized using Rq. This may be located at the following address:

3.3.2 Fluid Flow Solver

Flow is a mixed lubrication regime defined by the mean flow Reynolds method equation developed by Patir and Cheng (1978). This is a streamlined method for simulating the effects of surface roughness on partly lubricated contacts. The relationship between the pressure created by the lubricant and the current film thickness when their contact is rough is represented by this equation. Surface roughness has an impact on flow when the layer thickness regime is on the same order as the roughness. In this scenario, the average pressure between the surface and the lubricant is predicted by the average Reynolds flow equation [29], which is represented in equation (3.24). The average gap h is defined as the sum of the geometric compliance hg (explained in Section 3.2.1), the average unequal height of the piston and cylinder surfaces, and the resultant deflection and surface contact pressure. Because of elastic fluid mechanics. The formulae for leak stress and shear stress at the piston/cylinder contact have also been updated to include the "average flow rate." The next step is to assess each of the additional flow variables that have been incorporated to account for mixed lubrication. Appendix B offers analytical formulae discovered in the literature for these components, including those used to estimate viscous frictional force loss and leakage terms, while assuming isotropic surfaces with a Gaussian surface roughness distribution.

3.3.3 A sperity Contact Solver

The presence of surface asperity contact is the most critical feature of any mixed lubrication model. Surface roughness affects lubricant flows when gap heights reach the order of asperities. In addition to the elastic deformations induced by fluid pressure loading, the contact pressures generated assist in supporting the load in the gap and distorting the surfaces. Heat is also created via asperity contact and sliding.This model describes the roughness effect in two stages:

- Based on a contact model, a contact pressure distribution as a function of the local surface separation is given for the local event of an asperity contact.

- The effect of this asperity contact on the hydrodynamic pressure, deformations and heat transfer can be studied.

  Because this study assumes isothermal circumstances, the impacts of unequal heat generation and transmission are neglected. Given that complete film lubrication is expected to be present for the majority of pump cycles, this is acceptable.

  The alternative is because significant surface wear will limit the pump's life. Lee and Ren (1996) created a rough surface contact model based on the Boussinesq formulation, which describes the effects of elastic and plastic deformation of bumps as well as the impact of contact of one bump with neighboring bumps. This contact model is taken into account in this study. The model [30] is widely used to analyze contact irregularities in mixed lubrication of conformal surfaces [23, 34, 35].

  The contact calculations presented here are primarily based on surface topography (isotropic surfaces are considered) and material characteristics (material hardness, modulus, etc.). Furthermore, the contact equation holds true only if the projected average gap height is smaller than 1.5 times the surface roughness value. Rq.

3.3.4 Force Balance Solver

The unevenness shares the load in the area where the liquid film is present, which is an important factor to remember when modelling a mixed lubrication regime. It starts to disintegrate. As seen in Figure 24, the contact force functions in the same way as the corrective force section in the complete film FSI model (Equations (3.18) and (3.19). The equation for load balancing in the y direction is the same as equations (3.18) and (3.19), except that the compensatory pressure component pc is substituted with the bump contact

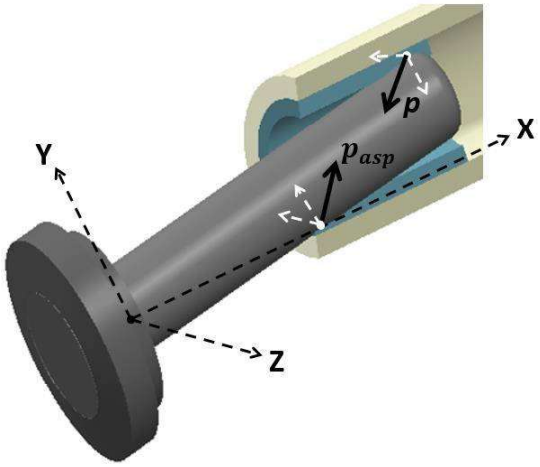

Figure24: Illustration of the fluid and asperity contact forces involved in load support during mixed lubrication conditions.

3.3.5 Solution Algorithm

Figure 25 depicts the solution algorithm for the hybrid FSI-EHD model. The approach begins similarly to the whole film FSI model by determining the beginning piston location and pinch speed. The average gap height across the interface, as well as the flow factor term used in the average Reynolds programme , are calculated. The average Reynolds equation for fluid pressures is solved, and these pressures are utilized to analyze the elastic deformation of the piston and cylinder surfaces .When the pressure-strain loop achieves convergence, the bump contact model of the contact pressure is solved when the area with the lowest gap height is anticipated. The piston force balance equation uses contact pressure load and fluid pressure to compute the piston pinch velocity at a given point in time until the outer loop converges. The squish velocity convergence value is utilized to determine the eccentric position of the piston at the next point in time by numerically integrating the squish velocity over time steps using Euler's explicit approach.

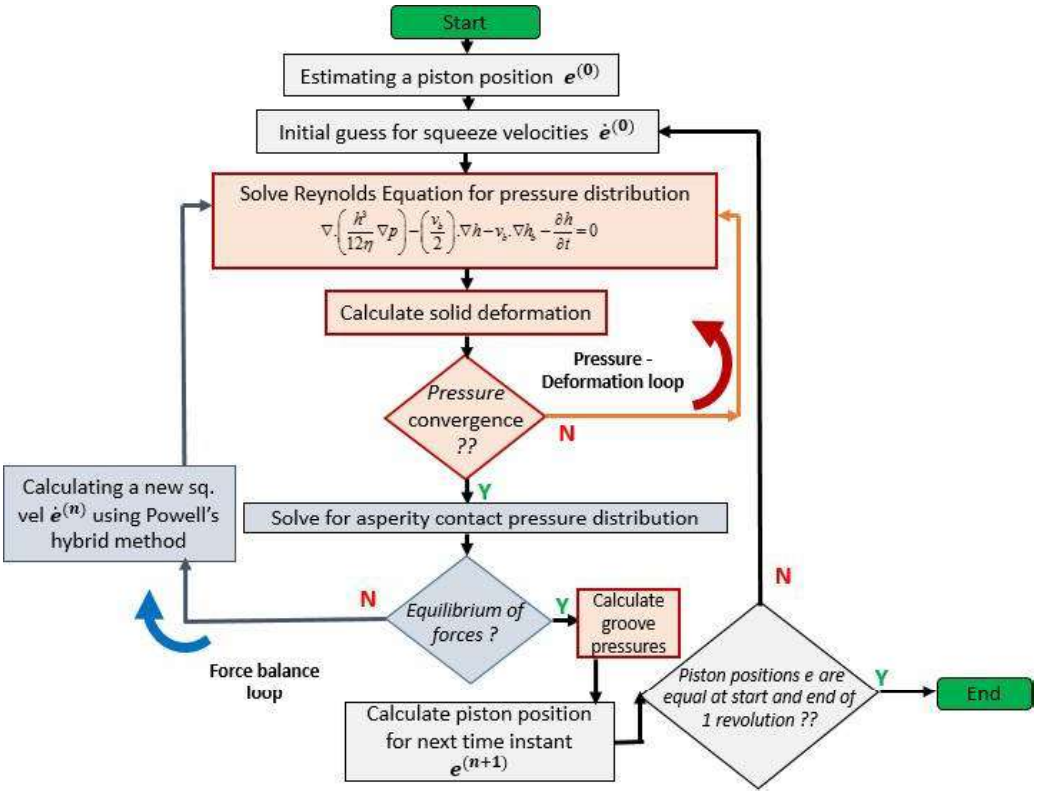

Figure 25: Algorithm for solving the Mixed FSI-EHD model at the piston/cylinder interface.

3.4 Line EHL Numerical Model for Friction Evaluation at the Cam/Piston Interface

This section explains the parameters of the numerical model created in [6], which was used to calculate the friction coefficient at each time step at the cam/piston interface. The ability to assess power losses caused by viscous friction at the cam/piston contact expands the model's capabilities greatly in this inquiry. Furthermore, this model was utilized in conjunction with the experimental technique developed (described later in Chapter 4) to examine the variation of the friction coefficient at the cam/piston contact for the reference machine.

As indicated in Section 3.2.5, the only side force acting on the pistons is the friction force created at the cam/piston contact interface. The friction between the cam and the piston, as well as the moment created by the cam's normal reaction to the piston, are the two origins of piston tilt.

3.4.1 Motivation for the Study of the Cam/Piston Interface

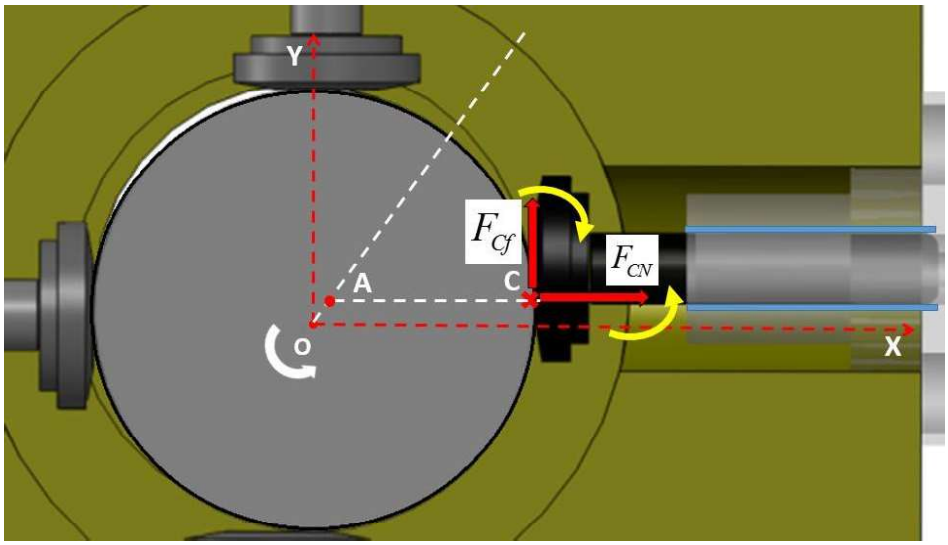

Figure26:The two sources of piston tilt are friction between the cam and the piston and the moment generated by the cam's typical response to the piston.

There are numerous strong reasons for conducting an in-depth examination of the cam-piston relationship. This interface must be designed to minimize friction between each cam and piston, resulting in less wear at the contacting surfaces during pump operation. Furthermore, the lubrication that exists between the cam's contact zone and each piston shears as the shaft rotates. This results in some non-negligible viscous shear losses, which affect total pump performance as well as unit efficiency. Another, and arguably the most important, reason to explore this interface is the change in friction force acting between the cam and each piston caused by dynamic loading at this contact during operation.

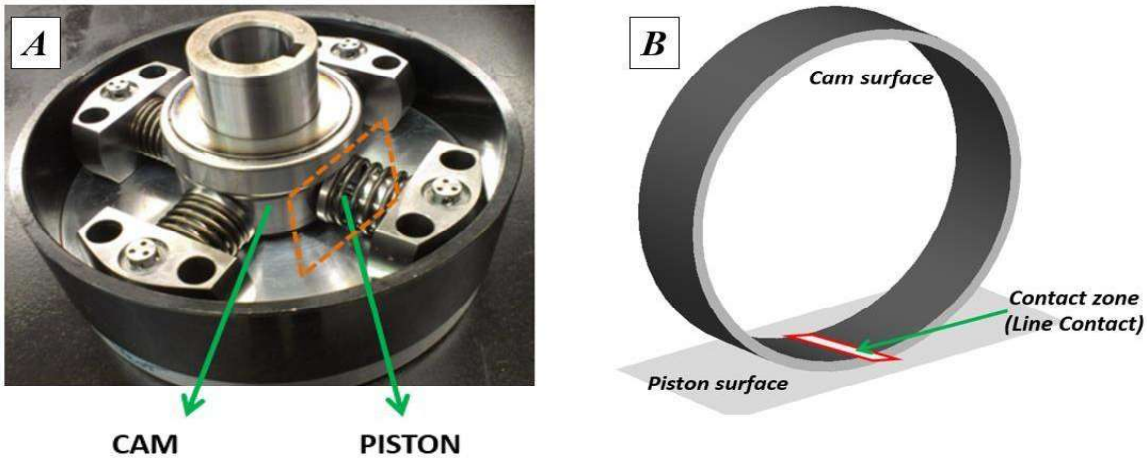

Figure 27: (A) Cam/Piston interface on the reference pump and (B) Illustration of the cam and piston surfaces causing a line contact.

There are numerous strong reasons why an in-depth analysis of the cam-piston interaction is essential. An successful design of this interface necessitates reducing friction between each cam and piston, resulting in reduced wear at the contacting surfaces during pump operation. Furthermore, the lubrication that exists between the cam's contact zone and each piston shears as the shaft rotates. This results in certain non-negligible viscous shear losses, which have an impact on total pump performance as well as the unit's efficiency. Another, and arguably the most important, reason to analyze this interface is the change in friction force acting between the cam and each piston as a result of the dynamic loading happening at this contact during operation.

The form of the contact zone between the cam and piston is similar to a line contact between a cylinder and a plane, as seen in Figure 27. The next subsections cover the whole approach used in the numerical model to predict the friction coefficient at the cam/piston contact under complete film lubrication conditions.

3.4.2 Governing Equations

At steady state (assuming that the load is completely carried by the fluid film), the pressure formed within the fluid film is sufficient to carry the contact load at the interface, resulting in the force-balance condition described below:

The density-pressure connection is represented by the Dowson and Higginson relation [61]. Using the Barus viscosity equation [62], it is possible to depict how viscosity changes with pressure in the fluid layer at this contact. Because the lubricant's viscosity increases substantially as it approaches the contact zone, this is a crucial factor in mimicking line contact at this junction.

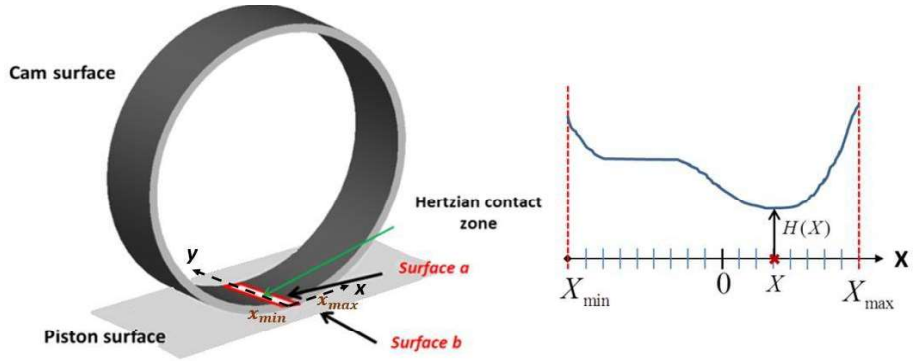

Figure 28: Lubricating gap domain discretized in the line contact with regard to the non-dimensional x- coordinate.

3.4.3 Non-Newtonian Fluid Behavior

The sliding motion that exists between the two surfaces at the point of line contact is one of the primary elements controlling frictional behaviour there. The two contact surfaces of the interface display pure rotating motion in ideal conditions, but large slip velocities can occur when the fluid approaches the contact zone in real-world scenarios. This can result in extremely high shear stresses, requiring the fluid to be considered as a non-Newtonian fluid. Radial piston pumps can have wide changes in rotating and sliding speeds at the cam / piston contact, necessitating the use of a flexible EHL line capable of producing an exact solution under all scenarios.When the Newton shear stress reaches the critical shear stress [see Figure 29], a simple non-Newton model [63] used in this investigation saturates. This permits the fluid to be classified as Newtonian unless the shear stress exceeds the shear strength. Slip happens at this moment, and the shear stress reaches saturation. Provide information on the non-Newtonian model that was employed.

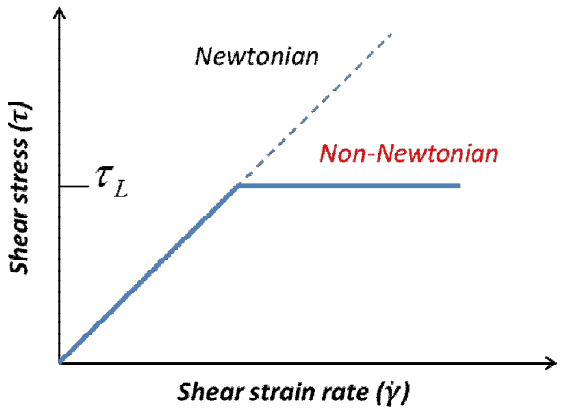

Figure29: Jacobson and Hamrock employed a non-Newtonian model. (1984)[63].

3.4.4 Numerical Solution Scheme

Use the Newton formulation stated in Eq. for pressure distribution (3.38). This intermediate pressure distribution is utilized to calculate the shear stress operating on both surfaces of the line contact, and the pressure value is changed using the non-Newtonian formulation. Elastic deformations of the two surfaces are detected and changes in the height of the surface gaps are estimated based on the new pressure distribution determined at each iteration. The new film thickness value is utilised to update the pressure field in the compression strain loop until both the fluid pressure and the film thickness value attain convergence.

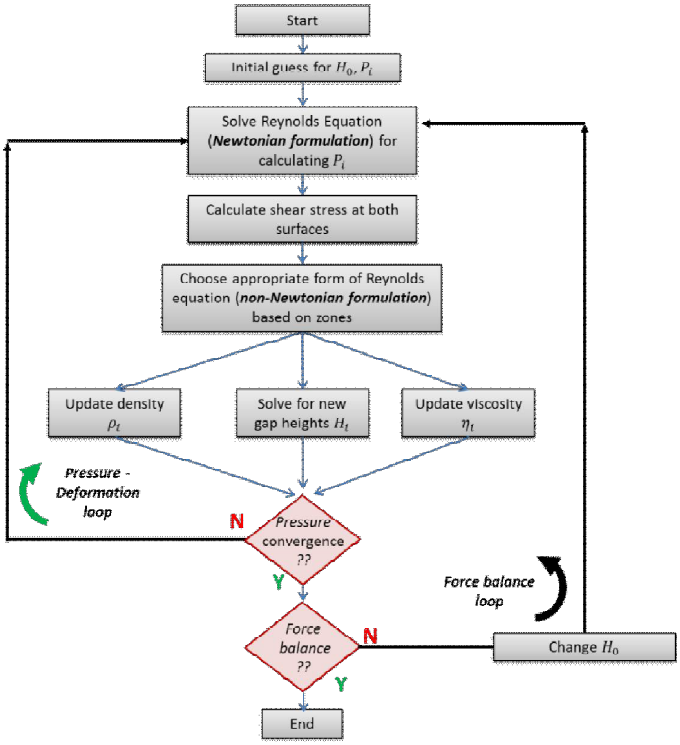

Figure30: Solution algorithm flow chart for the EHL line contact problem.

3.4.5 Viscous Friction and Power Losses at the Interface

The solution methods described here may create pressure distribution and film thickness in the lubricating domain. With the use of these numbers, the traction/friction forces acting between the surfaces may be determined. The bottom surface is subjected to shear stress (representative of the piston). The first term in the above equation reflects shear stress caused by the rolling component associated with surface velocities, whereas the second term represents shear stress caused by the sliding velocities of the piston (u1) and cylinder (u2) surfaces (represented in Figure 32).

The net friction force is produced by integrating the shear stress along the length of the contact zone. To calculate the friction coefficient, divide the traction force by the normal contact load at the interface.

CHAPTER 4.

INVESTIGATIONOFTHECAM/PISTONINTERFACE

The preceding chapter emphasized the need of precisely modelling the fluctuation of friction at the cam/piston interface in forecasting piston tilt behavior and, hence, power losses owing to leakages and viscous friction at the piston/cylinder gap. It was detailed how to estimate the friction coefficient at the cam/piston contact using numerical modelling, and the assessments of the friction coefficient that resulted for a variety of input parameters were displayed. To represent the friction at the cam/piston interface of an actual radial piston pump, however, exact inputs - namely, the dynamic circumstances of the contact load and cam and piston velocities - must be provided to the cam/piston numerical model.

Input variables needed to simulate friction at the cam/piston contact are listed in. While the load parameter W′ may be determined by examining the fluctuation of the contact loads on the cam from each piston, determining the velocity parameter use and the slide-to-roll ratio SRR is more difficult. The dimensionless material parameter G remains constant throughout (steel).

4.1 Previous Research into Friction at the Cam/Piston Lubricating Interface

Previously, two distinct cam/piston interface designs were investigated using the line EHL numerical model established [6]. Figure 31 depicts these two arrangements.

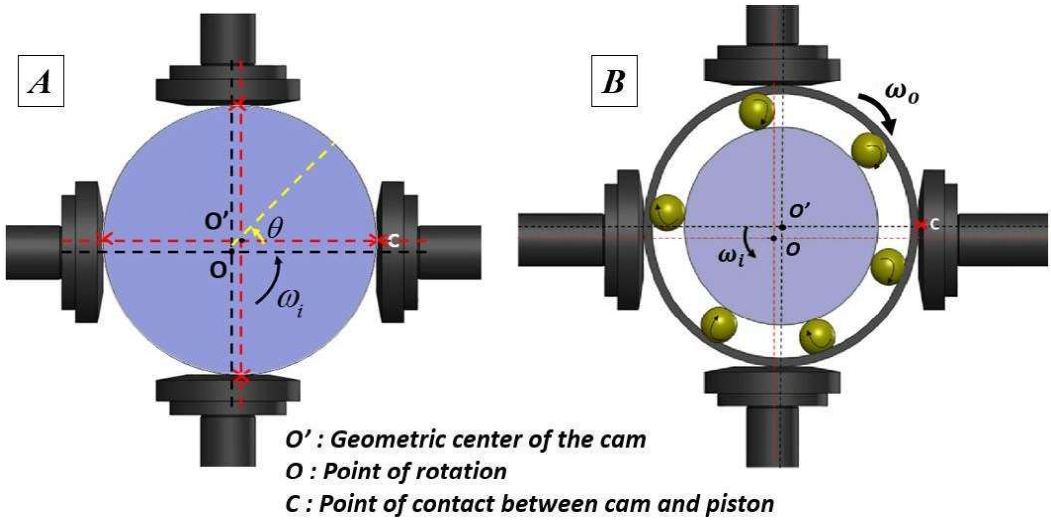

Figure31:The two cam/piston geometrical configurations analyzed in the past[6].

In the first case, the direct contact between the eccentric cam and each piston was analyzed to determine the change in friction during the duty cycle of the reference radial piston pump. At 700 bar outlet pressure and 1800 rpm shaft speed operating conditions, the results showed significant variations in the coefficient of friction (EHL viscous friction) during the pump cycle. However, a very low film thickness value ($<0.05\mu m$) is observed, indicating that there is considerable uneven contact between the cam and the surface of the piston. This indicates that the direct cam / piston contact configuration is not sufficient to lubricate this interface and therefore wears out with continuous service. The second case analyzed was about the reference geometry of the pump. In this design, roller bearings are provided between the inner eccentric shaft and the freely rotating outer race rest that contacts each piston. Since the outer ring rotates freely around its center, its angular velocity depends on the frictional force acting between the rolling bearing and the inner and outer rings. This requires an analysis of bearing dynamics in addition to the raceway-cage interaction, which is outside the scope of this study. A simplified approach was taken to model this interface, assuming that the contact between the outer ring and the piston with the highest instantaneous load is always pure rolling. Using this strategy, it was observed that the estimated entrainment rate was very low and the EHL model predicted inadequate pressurization of the fluid membrane. Therefore, in order to accurately predict the frictional, it is necessary to evaluate the driving speed existing at this contact interface. This chapter proposes a new experimental method for dynamically assessing the surface velocities of cams and pistons at any moment during shaft rotation. Therefore, a detailed analysis of the kinematics of the cam piston is required.

4.2 Kinematic Analysis of the Outer Race

Before starting the analysis of Cam kinematics, it is important to define the specific terms used in subsequent phases.

Drag Speed (): This represents the speed at which the lubricant flows into the contact area between the outer ring and each piston at any moment during one revolution of the shaft.

Slip Velocity (us): This represents the relative velocity between two surfaces in contact. H. Outer ring and each piston. Slip Roll Ratio (): This is defined as the ratio of slip speed to traction speed.

Where ($u1$) C and ($u2$) C are the top and bottom velocities with respect to the contact point [64] between the surfaces, as shown in Figure 32.

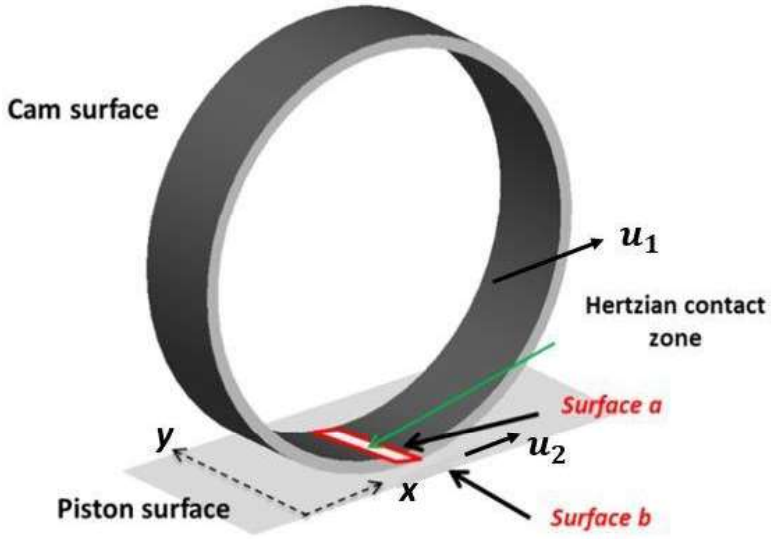

Figure32:The sliding velocities of the cam and piston surfaces are depicted in this illustration..

Figure 33 (A) depicts the cam-piston contact arrangement under consideration in this work, as well as the velocity diagram depicting the motion of various components. Using these kinematic relations, the equations for the instantaneous surface velocities of the outer race (u1) and piston (u2) at contact point C (shown in Figure 33 (B)), when viewed from a stationary frame of reference, are obtained.

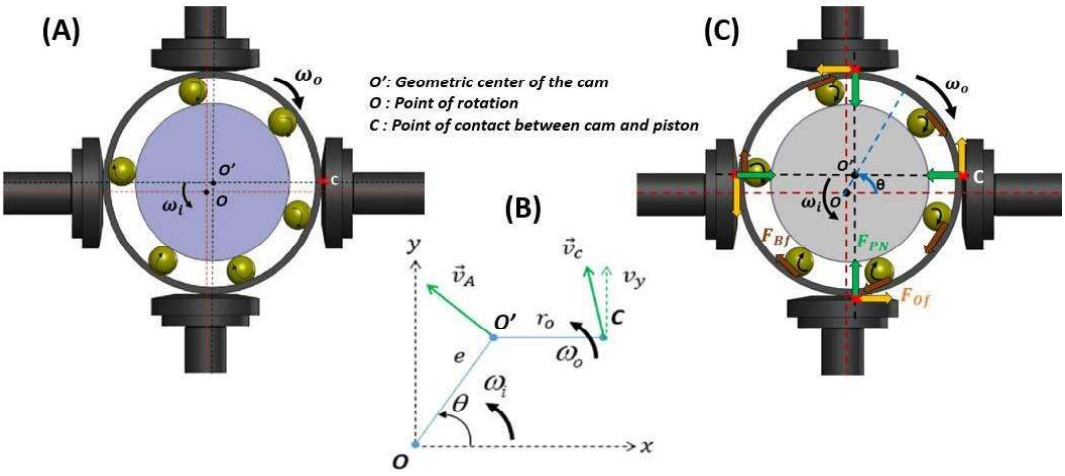

Figure 33: (A) Cam/piston interaction, including rolling element bearings and the outer race (B) Velocity resolution at the contact point; (C) Force diagram of the outer race.

4.1 The preceding equations show that the surface velocities are reliant on the angular velocity of the outer race (o), which is unknown. One way to express the outer race's moment equilibrium equations is as follows: According to the relationship shown above, the computation of this angular velocity depends on the friction force that each piston exerts, which might change as the shaft rotates. In addition, the intricate interaction with each of the rolling element bearings would have to be defined. As a result, an experimental measurement of the outer race velocity is regarded required to solve the problem. The most precise technique of producing input parameters for the friction model would be inferring these surface velocities from actual observations.

4.3 Experimental Study of the Instantaneous Velocity of the Outer Race

4.3.1 Experimental Setup

This section proposes experimental methods for assessing the surface velocity of the outer ring and each piston per revolution of the shaft. These surface velocities are used in equations (4.8), (4.9), and (4.10) to evaluate the input velocity parameters Ue and glide to roll ratio SRR of the numerical model. Figure 34 (A) shows the test setup used to perform this experiment. A fixed speed electric motor (set at 1800 rpm) rotates the eccentric shaft and the pistons of the radial piston pump move within their respective displacement chambers. The reference radial piston pump itself is screwed into the plate above the reservoir along with the hydraulic fluid. The same eccentric shaft passes through the gear pump. The gear pump acts as a pressure booster pump, supplying the radial piston pump

with a higher pressure (about 15 bar) of liquid than the environment. Since both pumps are encapsulated in the reservoir, how the ISO schematic in Figure 34 (B) actually exists in this test rig implemented at the Maha Fluid Power Research Center at Purdue University (USA). Is shown. The pressure relief valve is used to control the outlet pressure of the high voltage line.

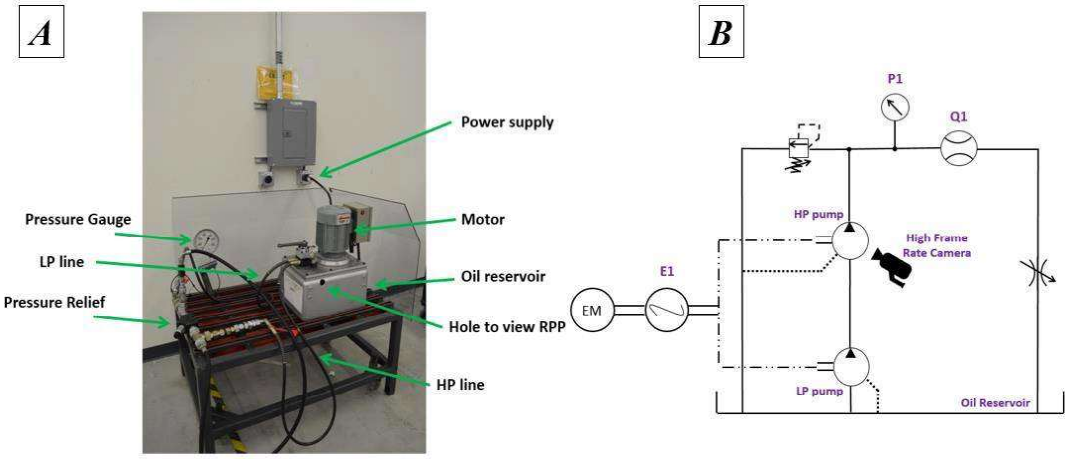

Figure 34: (A) Experimental test rig used to estimate the instantaneous angular velocity of the outer race,(B) Hydraulic circuit for the setup.

4.3.2 Proposed Methodology

A camera-based approach was tested to capture the instantaneous angular velocity of the outer ring as a function of shaft angle. As shown in Fig. 35 (A), the outer ring of the cam is painted black all around and has thin white stripes at regular intervals. The movement of the fine white stripes over one revolution of the shaft can be used to estimate the instantaneous angular velocity. To evaluate this with real-time pump operation, two holes had to be drilled. One is in the hydraulic oil reservoir housing and the other is in the radial piston pump housing. Custom-made mounting brackets have been manufactured to prevent hydraulic fluid from leaking through holes in the radial piston pump and to prevent the camera from obstructing the view of paint traces from the outside of the test bench. This is shown in Figures 35 (B) and 35 (C). They also show the display zone in which the camera is in focus to detect movement of the outer ring.

Figure35: (A) Painted outside race; (B) Custom bracket attachment utilized in test rig setup; and (C) Camera view during measurements.

Since the shaft rotates at a rate corresponding to 30 rev/s, a regular video cam which captures images at 30 frames per second (fps) is insufficient to capture the instantaneous velocity of the outer race. For this reason, a video camera was used which recorded images at the rate of 240 fps which corresponds to 8 frames being captured for a single rotation of the shaft. This allowed for 8 data points being available to analyze the instantaneous angular velocity of the outer race.

After the experiment was conducted, a post-processing methodology was used to analyze the velocity of the outer race by evaluating the position of each strip in every frame. A reference position was considered based on which the distance of each strip from this point was estimated as they entered the viewing area (seen in Figure 36 (A)). From thechangeinthedisplacementsofeachstripinaparticularframewithrespecttothepreviousframe ,theinstantaneousangularvelocity could be found .The presence of multiple thin strips with known values of the distance intervals between them were helpful in judging the displacement variation of each strip in successive frames. Many such frames were analyzed and a typical set of data of the instantaneous angular velocity of the outer race starting from when the first strip entered the viewing area up to when the last strip exited the view in area is shown inFigure36(A).

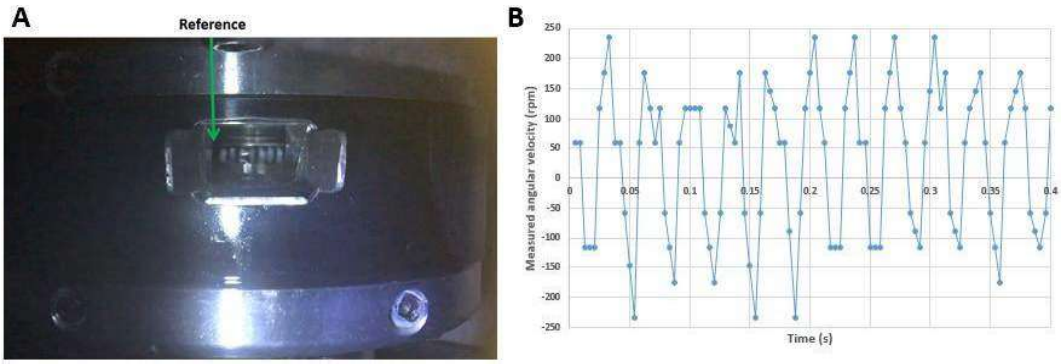

Figure 36: (A) Example of a single frame analyzed by estimating the distance of each strip from the reference location,(B)Typicalset of measured data points of instantaneous angular velocities obtained over multiple shaft revolutions.

To obtain the instantaneous outer ring velocity of a uniaxial rotation, the velocities were averaged at data points separated by 8 frame intervals. This allowed us to evaluate the momentary movement of the outer ring represented by the eight average data points of one rotation of the shaft during steady-state pumping. We used a cubic spline interpolation scheme to create a smooth curve to capture the instantaneous change in the angular velocity of the outer ring over the rotation of one shaft. Figure 37 shows the measured angular velocity of the outer ring interpolated over 360 ° of shaft rotation. Tests were performed on various pump operating pressures to understand the effect of the load present at the contact interface on changes in the angular velocity of the outer ring. This study considered a sufficient operating pressure range of 100 to 350 bar. The results obtained from these experiments were used in subsequent simulation studies under arbitrary operating conditions of the pump, as contact loads in this range were found to have no recognizable effect on the average velocity of the outer ring. However, this interpolated data does not take into account the fact that the shaft rotates eccentrically with each revolution. When assessing the actual angular velocity of the outer ring, this eccentric displacement present during shaft rotation must be subtracted from the measured data in order to obtain the correct movement of the outer ring movement. This eccentric displacement can be evaluated by considering the situation where the eccentric outer ring does not rotate around its own axis but rotates around its axis. This shows the movement of the circle at two time points (centers A and B) that rotate around the fixed position of space O in Fig. 38 (A). The offset above is the distance subtracted from the measured position data. With this shift taken into account, the actual change in angular velocity can be plotted as a function of the shaft angle, as shown in Figure 38 (B).

This is an interpolated 4-cycle chart because the movement of the outer ring is affected by the 4 pistons that exist. You can see that the curve appears to pass through almost all of the eight points obtained in the experiment.

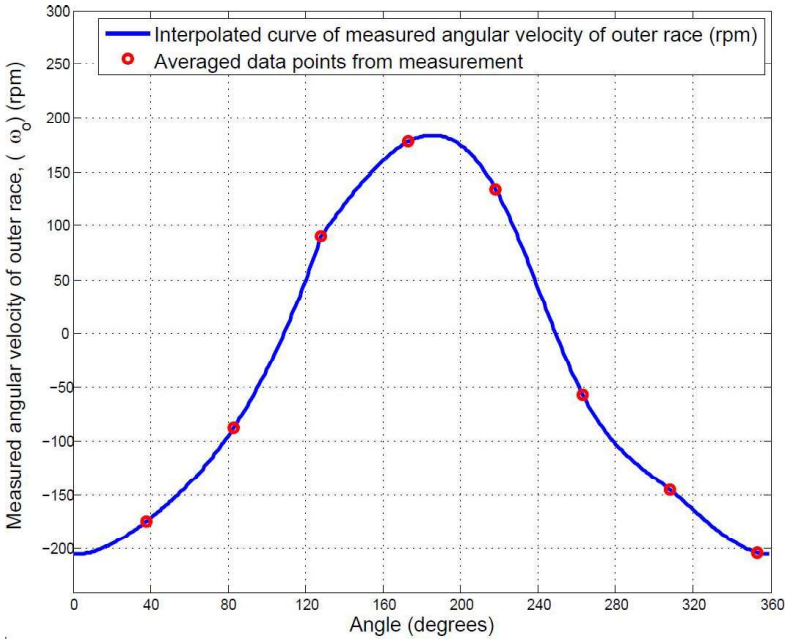

Figure37: Curve generated from them ensured velocity of the outer race through an interpolation of the measured data points over one shaft revolution.

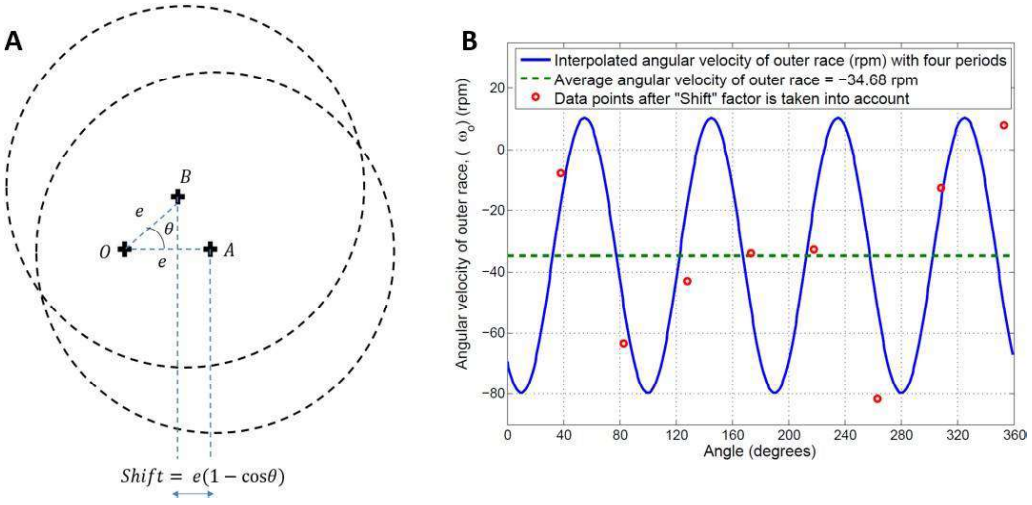

Figure 38: (A) Shift owing to eccentricity, which must be removed from the experimentally recorded angular velocity; (B) Actual change of the outer race's angular velocity as a function of shaft angle.

In this way, the variation of the outer race's rotational velocity may be determined and utilized as the last input parameter for the friction model presented in the previous chapter.

4.4 Numerical Evaluation of the Friction Coefficient at the Cam/Piston Interface

Input parameters are displayed in Figure 39 for the evaluation of the friction coefficient at the cam-piston interface. The outer race's angular velocity was utilized to calculate the entrainment velocity input parameter Use from Equation (4.8). Figure 40 illustrates how the shaft angle affects the fluctuation of the friction coefficient (A).

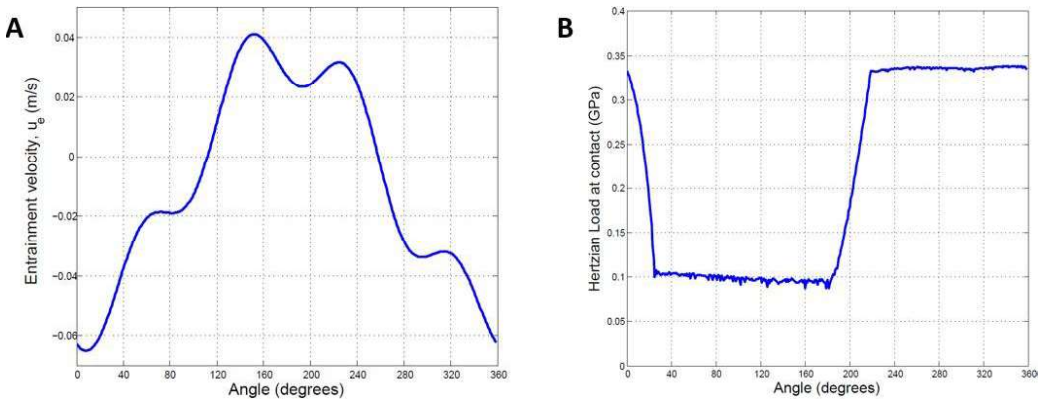

Figure 39:Pump outlet pressure: 700 bar, Shaft speed: 1800 rpm. Entrainment velocity (A) and Hertzian load (B) at the contact interface

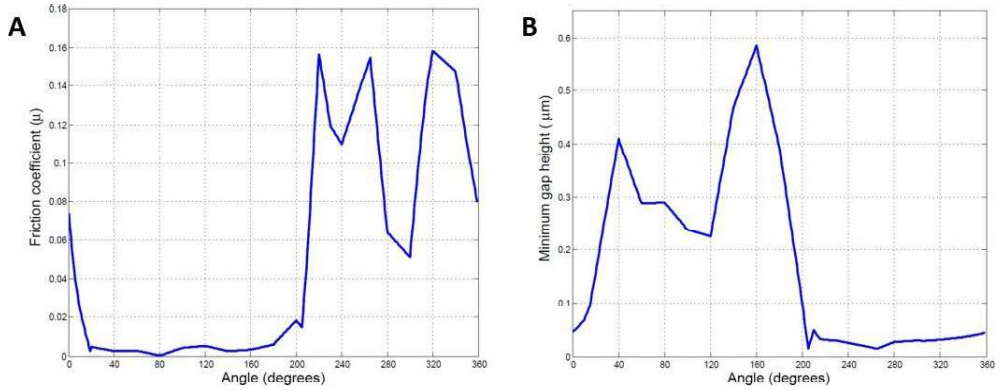

Figure40:Pump outlet pressure: 700 bar; shaft speed: 1800 rpm; outputs from the EHL friction model. (A) Variation in friction coefficient over one pumping cycle, (A) Variation in minimum gap height at the interface over a pumping cycle.

The friction coefficient during the suction stroke (0o to 180o) of one pumping cycle is projected to be of the order of 0.001, although it seems to be on the order of 0.1 during the discharge stroke (180o to 360o) from the perspective of the outer race. The greater magnitude of the friction coefficient during the discharge stroke tends to imply that the

lubricating regime may no longer be complete film lubrication. Figure 40 (B) shows that the smallest gap height observed is projected to be less than 1 m during the pumping cycle at steady state.

4.5 Model Validation :An Indirect Empirical Approach

An indirect technique including a force and moment analysis of the cam's outer race is developed to confirm the results of the friction coefficient fluctuation between the outer race and each piston as a function of shaft angle. Figure 41 displays the many factors at work on the outer race. Because the frictional forces caused by the ball bearings are not represented throughout the study, they are found to be the sole unknown in Equation (4.11). By solving this equation, the coefficients of frictional force owing to ball bearings derived (from Figure 41) are compared to realistically observed values in real-life

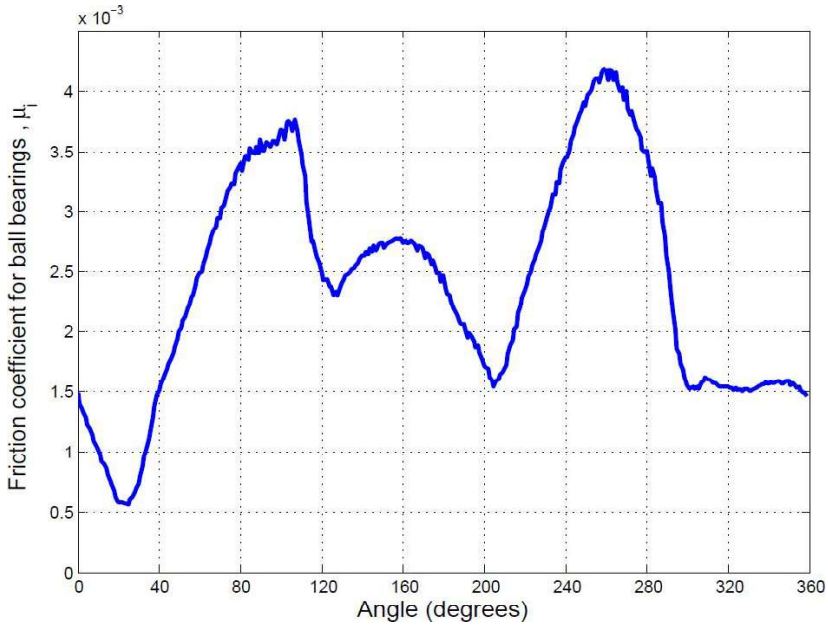

Figure41:Variation of the friction coefficient with shaft angle as obtained from solving the moment-balance equation of the outer race.

As illustrated in the figure, the range of values obtained for the friction coefficient due to ball bearings for one revolution of the shaft (0.0005 0.0043) appear to satisfy physically realizable estimates for the same (typically of the order of 0.001) during efficient bearing operation at steady state. As a result, this indirect technique to validating the entire cam-piston interaction model is adequate.

4.6 Results from the Fully-Coupled FSI-EHD Pump Model

The findings of the fully-coupled model are discussed in this section. The complete film FSI-EHD model of the piston/cylinder interface is combined with the EHL friction model of the cam/piston interaction in this case. The specifics of the design input variables utilized to produce all the simulation results for the reference pump design covered in this section are provided in Table 2.

Table2: Design input parameters for there paused in the simulation results.

PARAMETER	DESCRIPTION/ VALUE
DISPLACEMENT	1.0CC/REV
NOMINALCLEARANCEBETWEENPISTONANDCYLINDER	8 μm
WORKINGFLUID	ISOVG32HYDRAULICOIL
DENSITY@ 15°C	869KG/M^3
VISCOSITY@15°C	0.02PA-S
PISTON&CYLINDER MATERIALS	STEEL
YOUNG'SMODULUS	210GPA
POISSON'SRATIO	0.29
DENSITY	7850KG/M^3

.

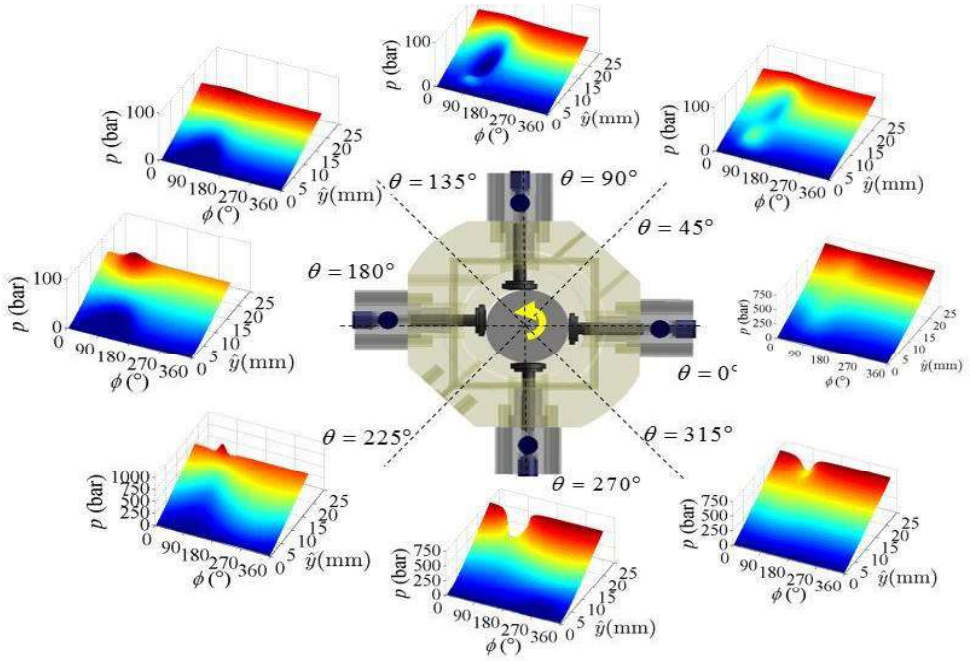

Figure42:Unwrapped pressure field in the piston/cylinder gap domain over one shaft revolution for Pump outlet pressure:700 bar, Shaft speed: 1800rpm

4.6.1 Pressure Profile sand Gap Height Distributions

Figures 42 and 43 show the changes in pressure field and gap film thickness in the lubrication gap region over one shaft rotation when the described FSI solution algorithm converges at a pressure of 700 bar at the outlet and a shaft speed of 1800 rpm. I am. .. The pressure profile shown in Figure 12 in displacement space is used as a boundary condition. The fields shown are for a single piston / cylinder pair. They are shown in an unwrapped configuration. Where ∅ represents the angle of circumference and ŷ is the length of the gap along the axis of the cylinder. Also, θ represents the shaft angle, which is the angle at which the eccentric cam rotates, and θ = 0o is the position of the piston when at BDC (start of suction stroke). From these numbers, there is a lower pressure during the suction stroke (θ = 0o − 180o) and a higher pressure buildup in the displacement chamber during the pressure stroke (θ = 180o − 360o). Gap pressure. Also, depending on the tilt position of the piston, there are peaks or valleys of pressure in areas of the cylinder where the height of the gap is small, which is a characteristic effect of squeezing the liquid film.

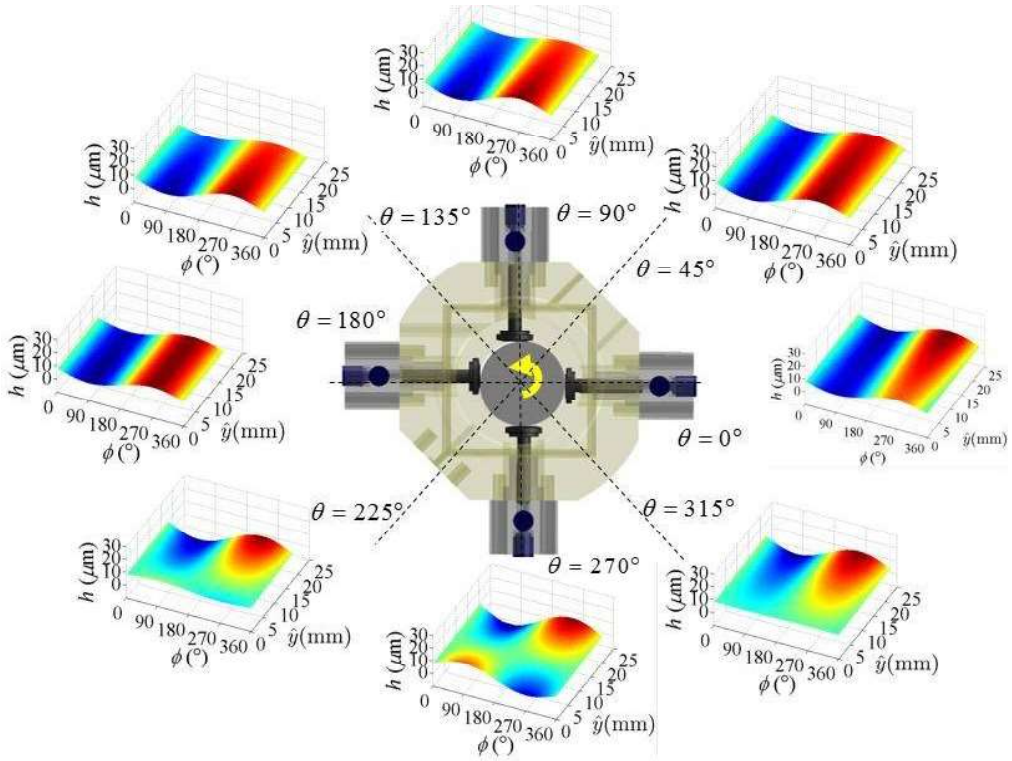

Figure 43: Unwrapped film thickness configuration in the piston/cylinder gap domain over one shaft revolution for Pump outlet pressure: 700bar, Shaftspeed:1800rpm.

4.6.2 Effect of Incorporating the Cam/PistonFriction Modelon Piston Tilt

As already mentioned, the fully coupled FSI-EHD pump model is an extension of the work presented in [6]. Since there is no verified cam / piston model, we assumed the coefficient of friction between each piston and the outer ring of the cam. A constant coefficient of friction of $\mu = 0.1$ was assumed. This represents a pure sliding contact between the two steel surfaces (Fig. 44 (A)). We also assumed that the outer ring always rotates in the same direction as the shaft during the pump cycle (Fig. 44 (B)). Under these assumptions, the tilt of the modeled piston was found to be very different compared to the current behavior observed by the fully coupled algorithm (Figure 45).

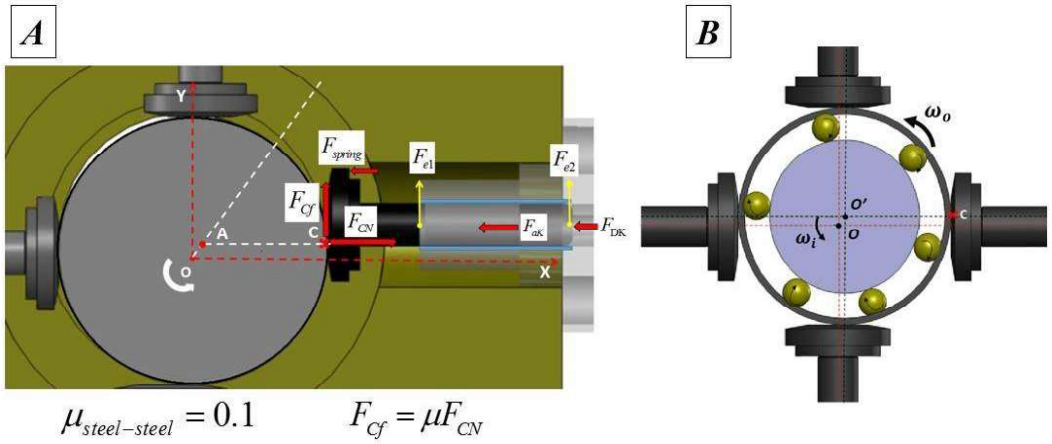

Figure 44: (A) Previously made assumption of the non-varying friction coefficient at thecam/piston interface, (B) Assumption for the rotational direction of the outerrace (sameas the direction ofthe shaft).

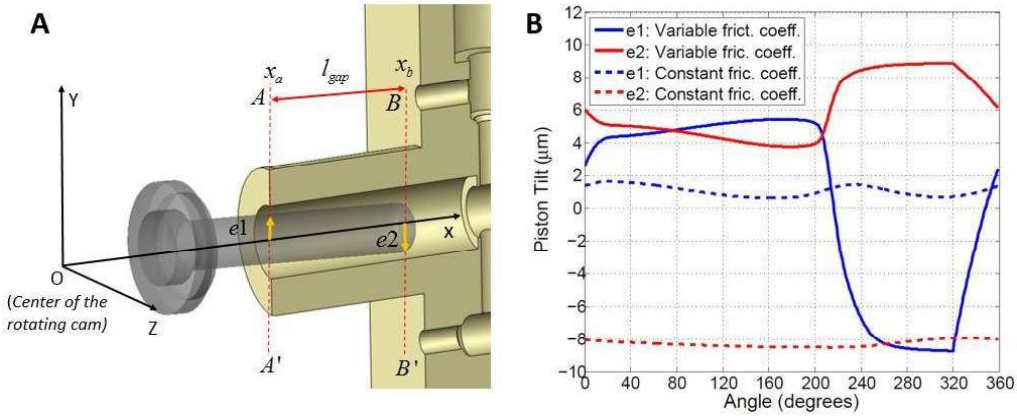

Figure 45: Comparison of the piston tilt behaviours of the constant cam-piston friction coefficient assumption model versus the changing friction coefficient model throughout one shaft rotation for Pump outlet pressure is 700 bar, and the shaft speed is 1800 rpm.

Based on the data in Figure 45 (B), it is possible to deduce that the fluctuation of the friction coefficient as well as the direction of rotation of the outer race during each shaft revolution at steady state are critical aspects to consider when designing a rotating cam type radial piston machine. These factors are also important in determining the degree and location of probable solid contact between each piston and cylinder during the pump cycle.

4.6.3 Effect on Pump Performance

Figure 46 shows the fluctuation of leakage in a single piston/cylinder gap throughout a single shaft rotation. Because there is a bigger pressure differential between the displacement chamber end and the pump case during the delivery stroke (= 0o 180o), it is evident that there are substantial leakages via the gap at this time. The mean leakage flow rate for the pump at each operating state may be calculated by adding all leakages at all four piston/cylinder interfaces and averaging across a pumping cycle. Figure 47 depicts the fluctuation in viscous friction power loss at each piston/cylinder interface over the course of one pumping cycle. Following the same reasoning as previously, a greater gradient in the pressures between the displacement chamber and the case results in larger values of the viscous friction forces present in the gap, resulting in more viscous power losses across the gap. Overall viscous power losses are computed in the same way that leakages are evaluated.

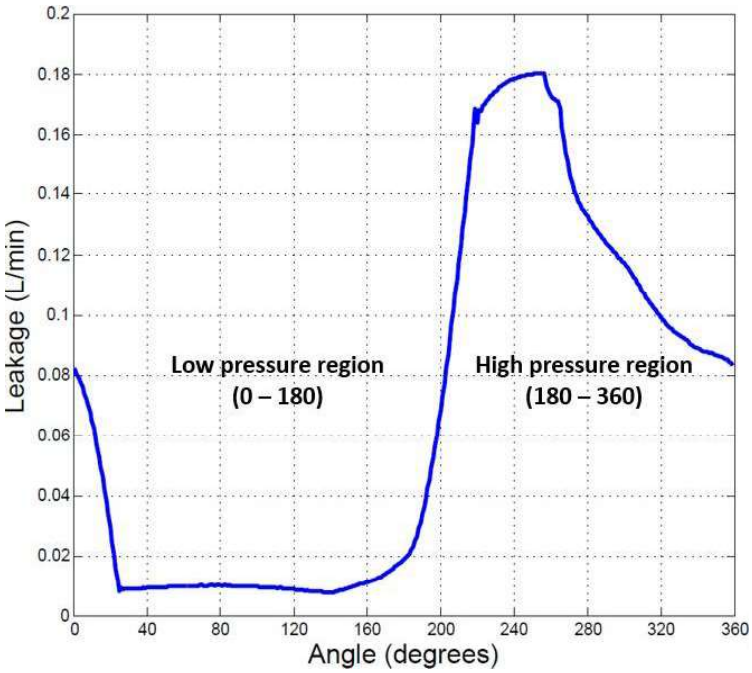

Figure46:Variation of piston/cylinder interface leakage as a function of shaft angle for Pump output pressure: 700 bar, Shaft speed: 1800 rpm.

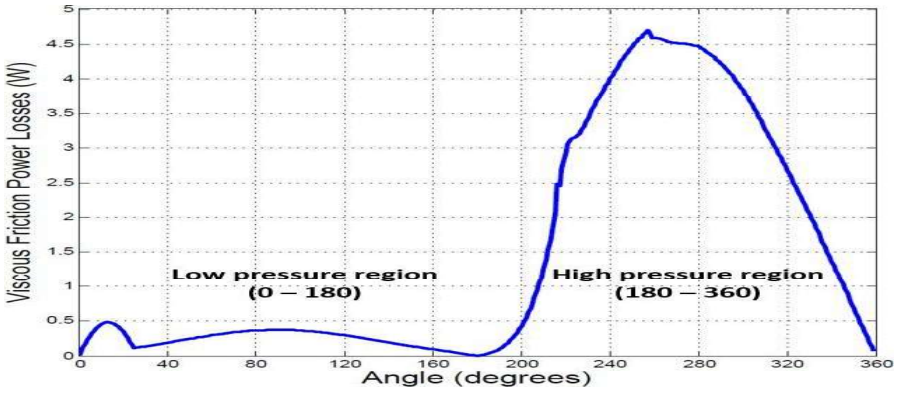

Figure 47: Variation of viscous friction power losses at the piston/cylinder contact as a function of shaft angle at pump outlet pressure of 700 bar and shaft speed of 1800 rpm.

A fixed speed motor is used to drive the reference unit at its nominal speed of 1800 rpm, for which measurements of the outer race velocity were available as previously reported. In three working circumstances, the outlet pressure was changed while the shaft speed was maintained constant at 1800 rpm. Volumetric efficiency of the pump is examined in two cases: when the cam/piston interface model is utilised and when a constant friction assumption is adopted (Figure 48). Figure 49 depicts power losses due to viscous friction at the piston/cylinder and cam/piston interfaces for all operating states. The pump's four piston/cylinder interfaces were all tested.

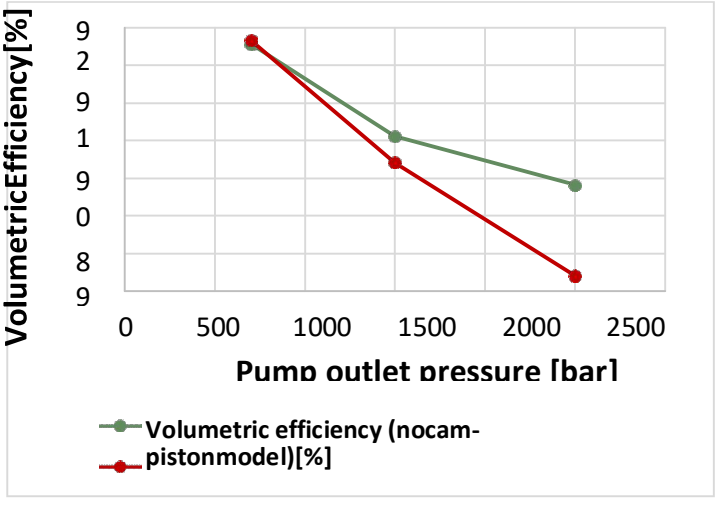

Figure 48: Comparison of the volumetric efficiency calculated for the Pump output pressure using the constant cam/piston friction coefficient assumption model and the variable friction coefficient model: Shaft speed: 1800 rpm, 700 bar.

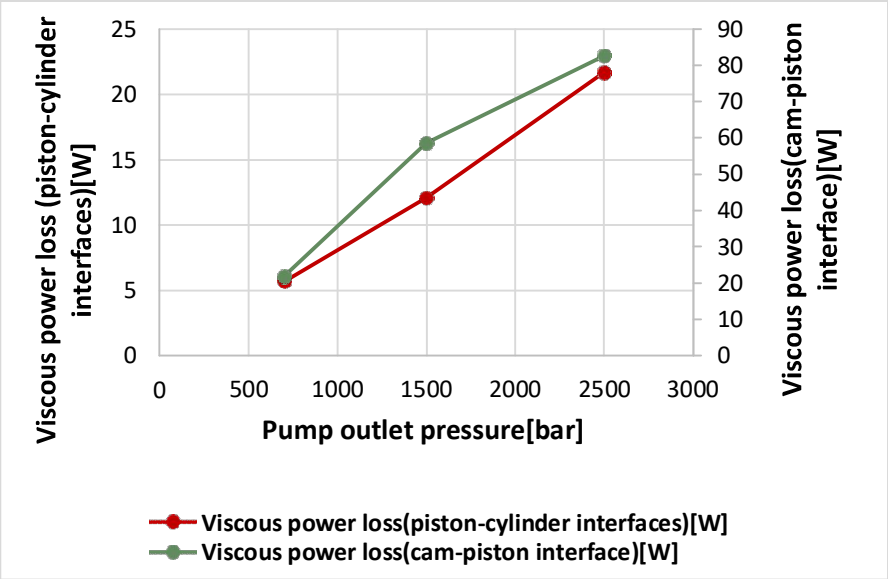

Figure 49: The viscous power losses at the cam/piston and piston/cylinder interfaces were compared using the constant cam/piston friction coefficient assumption model and the variable friction coefficient model for Pump outlet pressure: 700 bar, Shaft speed: 1800 rpm.

By considering the cam / piston interface, the behavior of the piston tilt also affects the amount of leakage at the piston / cylinder interface, thereby achieving the volumetric efficiency accuracy expected for the engine under different operating conditions. It is clear that it will have an impact. This can be seen in Figure 48, where a significant difference in volumetric efficiency is predicted, especially at ultra-high pressures (2500 bar). We also find that the power loss due to the viscous friction loss present at the cam / piston interface is very important. This is even greater than the loss that exists at the piston / cylinder interface for each revolution of the shaft (as shown in the figure). 49). The full film piston / cylinder gap assumptions are used to make the comparisons shown in this section. This is done to demonstrate the importance of accurately assessing the variation in the coefficient of friction at the cam / piston interface with respect to piston tilt and gap performance. The importance of the mixed lubrication assumption at the piston / cylinder interface will be demonstrated later using the results obtained.

CHAPTER 5.
POTENTIAL OF THE FULLY-COUPLED FSI-EHD MODEL ININVESTIGATING THE EFFECT OF CIRCUMFERENTIAL PISTON GROOVESON LUBRICATING PERFORMANCE

This chapter introduces the possibilities of fully coupled models developed for the design of efficient and durable radial piston machines. Two aspects of efficiency and durability were the ultimate goals of this study, and to achieve these goals, we analyzed the surface features, the effect of the circumferential piston groove.

Two key operating conditions were considered when performing all the analyzes presented in this chapter. They are shown in Table 3. The reason for studying these two specific operating conditions is primarily to improve the design of the reference machine to achieve very high operating pressures (> 700 bar).

Table3: Operating conditions at which the features of there ference designis examined.

Outlet Pressure [bar]	***Shaft Speed [rpm]***
700	*1800*
2500	*1800*

5.1 Investigating Grooved Piston Designs

The main motivation behind the introduction of surface features such as the circumferential groove of the piston is that the groove allows for a region of constant lubricating oil pressure, which affects the tipping of the piston and ultimately between the metals. The surface of the piston and cylinder is to prevent wear due to contact. This technique for modeling the effect of grooves has been used in various applications in the past [48-50]. The next section details how the location and number of piston grooves affect pump wear and performance. Several case studies were conducted to investigate the effect of circumferential piston grooves on hydrodynamic effects, as well as piston tilt during operation (wear due to metal-to-metal contact). Figure 50 shows the case considered. A 2D unwrapped fluid mesh constructed for each of these cases is also shown.

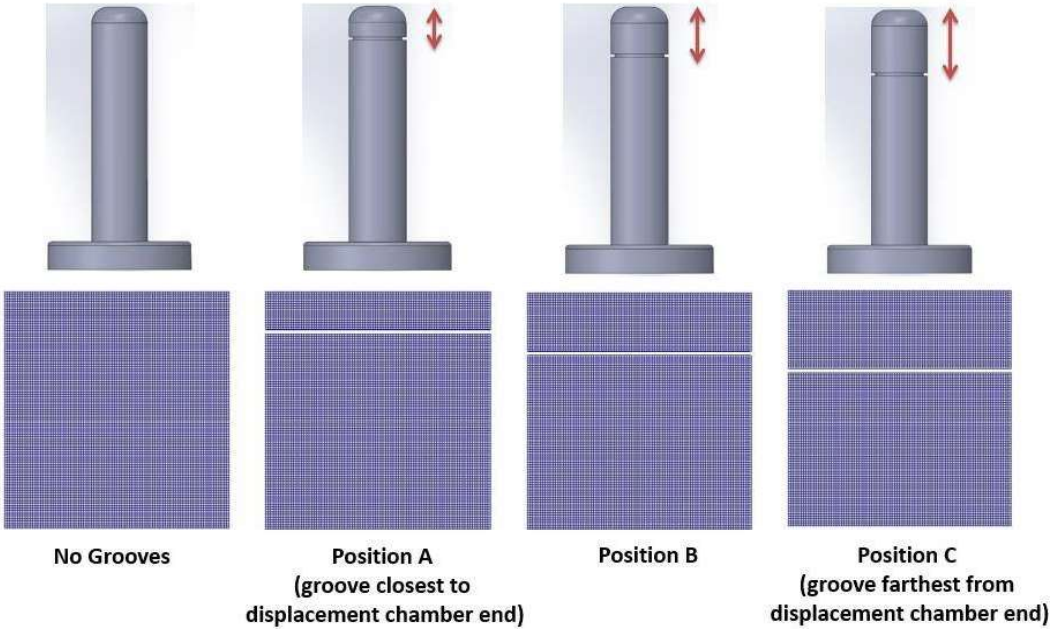

Figure50: Groove configurations on the piston studied with respect to position.

The modelling strategy used to determine the pressure inside these grooves has been demonstrated in Section 3.2.2. The pressure within each groove is determined to be the same along the specific groove surface using the control volume technique outlined. Figure 51 depicts the pressure fluctuation within the groove at Position 'A' throughout a single pumping cycle. Figure 52 also depicts the variation in flow rates coming into this groove from each side as the shaft revolves. The measured flow rates tend to normalize in amplitude as they enter the groove from either side, as seen in the picture.

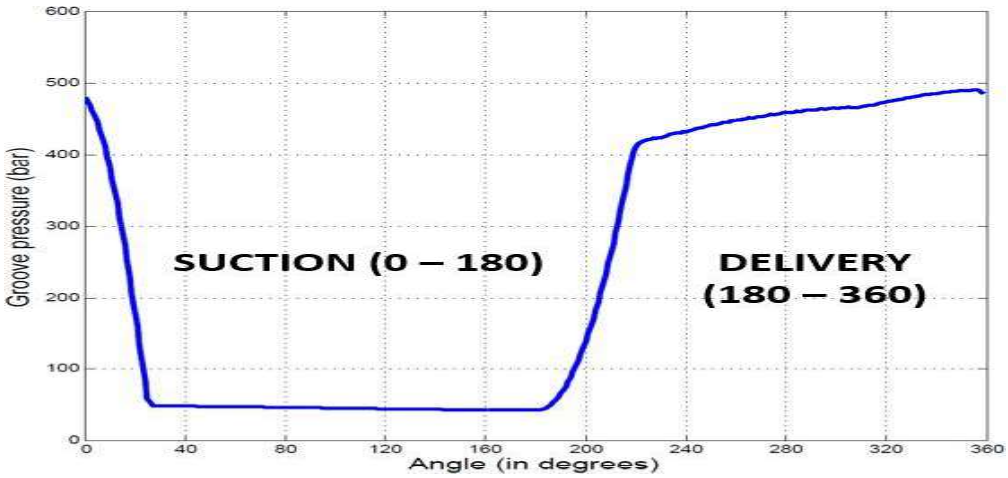

Figure51:Pressure variations in the groove (at Position 'A') as a function of shaft angle for Pump outlet pressure: 700 bar, Shaft Speed: 1800 rpm

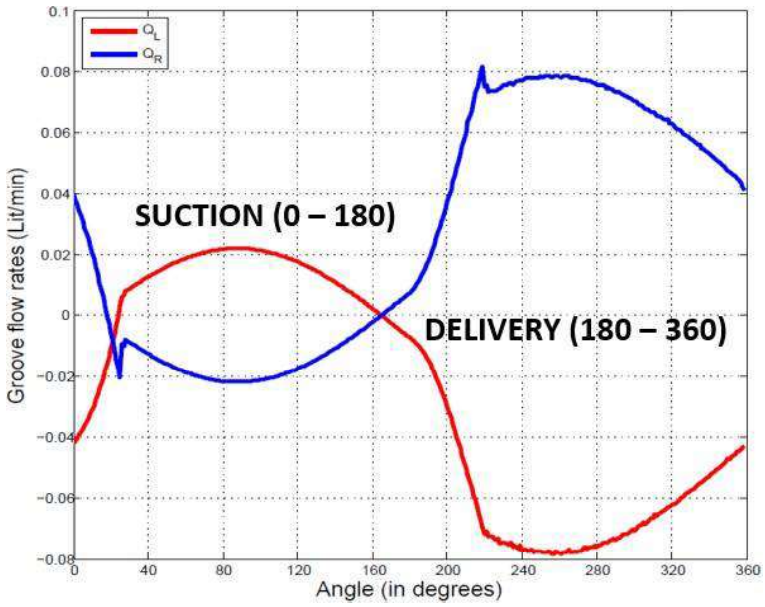

Figure52:Flow rates entering the groove (at Position 'A') from each side vary as a function of shaft angle for Pump output pressure: 700 bar, Shaft Speed: 1800 rpm.

To understand the influence that the position of a single groove can have on piston tilt, comparisons are done between the reference pump utilizing grooved pistons with the groove position altered and the reference pump using pistons without any grooves. The findings of such comparisons are discussed in depth in the next section.

5.2 Significant Results

5.2.1 Effect of Grooves on Piston Tilt and Hydrodynamic Effect

The first significant factor to evaluate is whether the existence of a groove impacts the hydrodynamic effect produced by the pump during operation. This may be investigated by thoroughly examining the various components in the Reynolds equation, which is used to solve for the pressure distribution inside the fluid.

To analyze the hydrodynamic effect, two cases—the first utilizing pistons without grooves and the second using a piston with one groove at Position 'A'—were carefully examined (Figure 50).

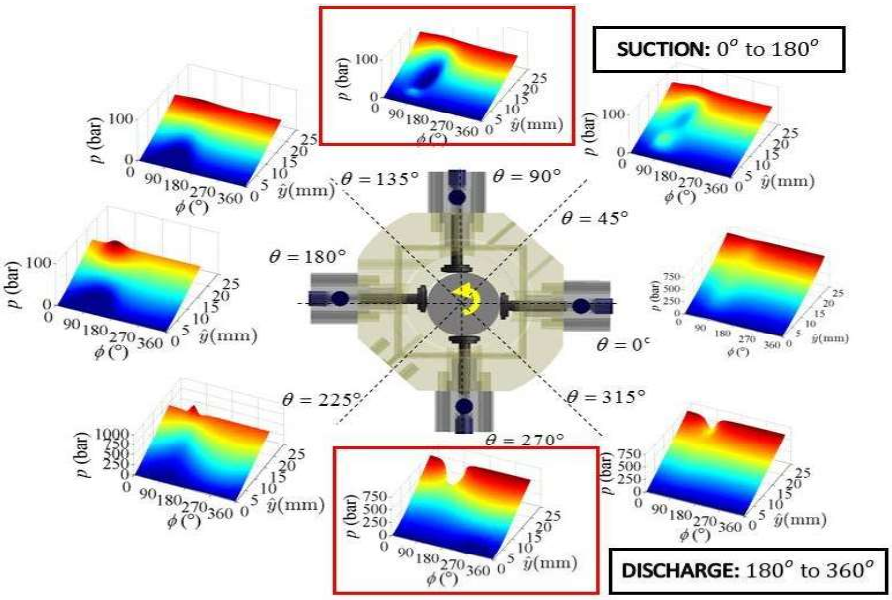

Figure 53: Instantaneous pressure field in the lubricating gap domain over one shaft revolution obtained using the piston/cylinder FSI-EHD model for Pump outletpressure:700 bar, Shaft speed: 1800 rpm.

The balance changes in the case of Groove Position 'A' as compared to the case without any piston grooves. This is better demonstrated by examining which components in the Reynolds equation are most influenced by the existence and position of a groove, i.e. the Reynolds equation terms that lead to an increase in hydrodynamic pressure production. The Reynolds equation terms are evaluated for two positions - one during the suction stroke (0o to 180o) and one during the discharge stroke (180o to 360o) - throughout a single shaft revolution. Figure 53 displays the instantaneous pressure profile for the two

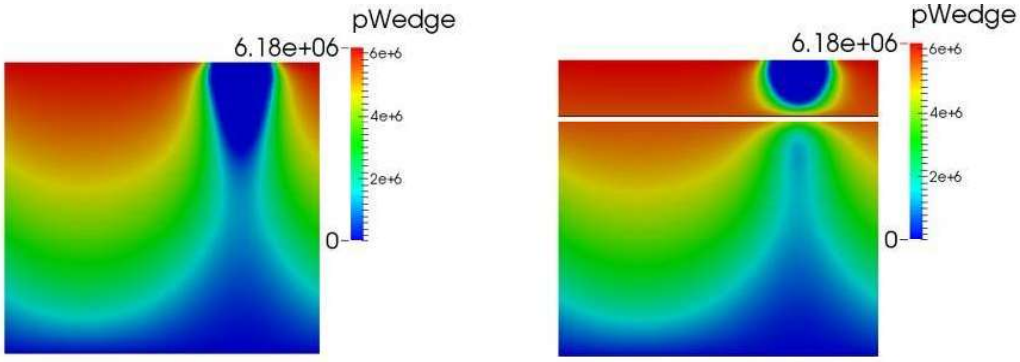

instants investigated.

Figure 54: Comparison between the pressures generated from the wedge effect for the case of a piston with no grooves (left) and a piston with grooves at PositionA(right) during one instant of the suction stroke.

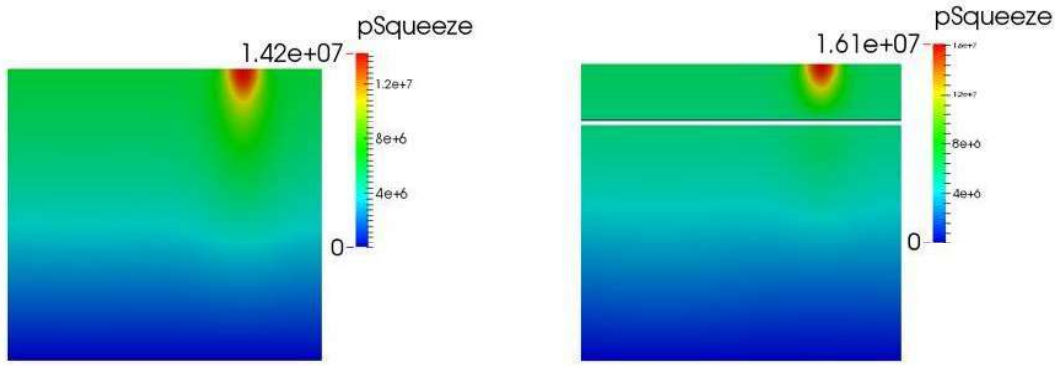

Figure55:Comparison of pressures created by the usual squeezing effect for a piston with no grooves (left) and a piston with grooves at Position A (right) during a single suction stroke moment.

During the piston's suction stroke, the hydrodynamic pressure generation is boosted by an increase in the pressure created by the Normal Squeeze and Physical Wedge effects.

Figure 54 shows that the amplitude of pressure caused by the wedge effects is greater, particularly in the area surrounding the groove. In the case of a piston without grooves, the blue and green portions that represent lower pressure regions are replaced with the red regions that represent significantly greater pressures. Through a consideration of the normal squeeze effect in Figure 55, for both piston situations, the same effect of producing an area of continuous pressure of greater magnitude surrounding the groove can be shown. An examination of the normal squeeze effect in Figure 55 shows the same impact of producing an area of continuous pressure of greater magnitude around.

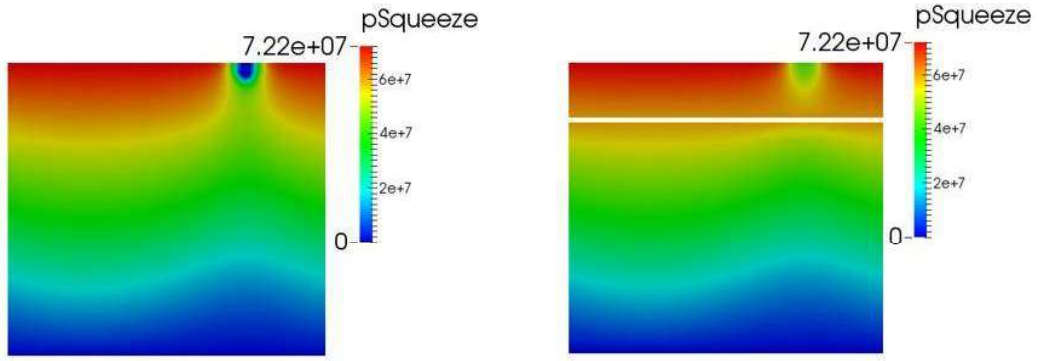

Figure56:The pressures created by the usual squeezing effect for a piston with no grooves (left) and a piston with grooves at Position A (right) during one instant of the discharge stroke are compared.

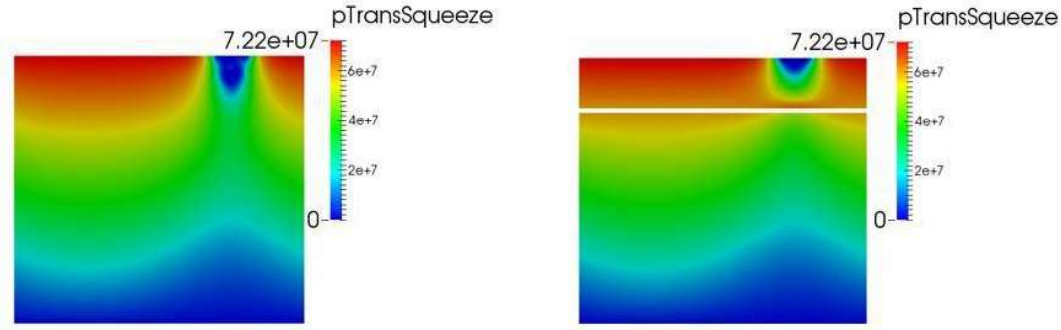

Figure 57: Comparison of pressures created by the translational squeezing effect for a piston with no grooves (left) and a piston with grooves at Position A (right) during one instant of the discharge stroke.

A similar phenomenon is observed in the exhaust stroke of the piston each time the shaft makes one revolution. In this case, the terms that play an important role in increasing the total hydrodynamic pressure generation in the gap are the normal and translational compression terms of the Reynolds method. Figure 56 shows the area of high pressure (red) due to the normal squish effect surrounding the groove compared to the case of a groove less piston (yellow and green pressure at the same location). The same applies to the pressure generation due to the translational compression effect of the two cases at the same moment of the discharge stroke analyzed in Figure 57.

Therefore, it can be seen that in the specific case of the groove position "A", the balance of the piston can be changed by enhancing the hydrodynamic effect caused by the position of the groove as compared with the case without the groove.

5.2.2 Piston Balance and Investigating Piston/Cylinder Contact

Grooves have been shown to affect the balance of the piston. However, the position of the groove can affect whether the piston balance is improved and whether the load is completely carried by the fluid film. For this reason, consider a reference pump that operates on pistons in different groove positions (positions "A", "B", "C"), assuming full film lubrication conditions with EHD effects. As shown in the figure, the change in the magnitude of the artificial contact load applied to maintain the stability of the numerical method is investigated for each case over a single pump cycle at a pump outlet pressure of 2500 bar and a shaft speed of 1800 rpm. To do. 58 During one cycle (20 *o* to 60 *o* and 180 *o* to 210 *o*), if there is no groove, the contact between the piston and cylinder will occur for a long time, while this contact will be the closest single groove. In the case of, it

can be observed that there is a significant decrease. The end of the displacement chamber of the piston (groove position "A" in Figure 50). Here, the contact appears to be short-lived (180 *o* to 210 *o*), and the magnitude of the contact also appears to be diminishing. This is very important as the wear that can occur due to this metal-to-metal contact is

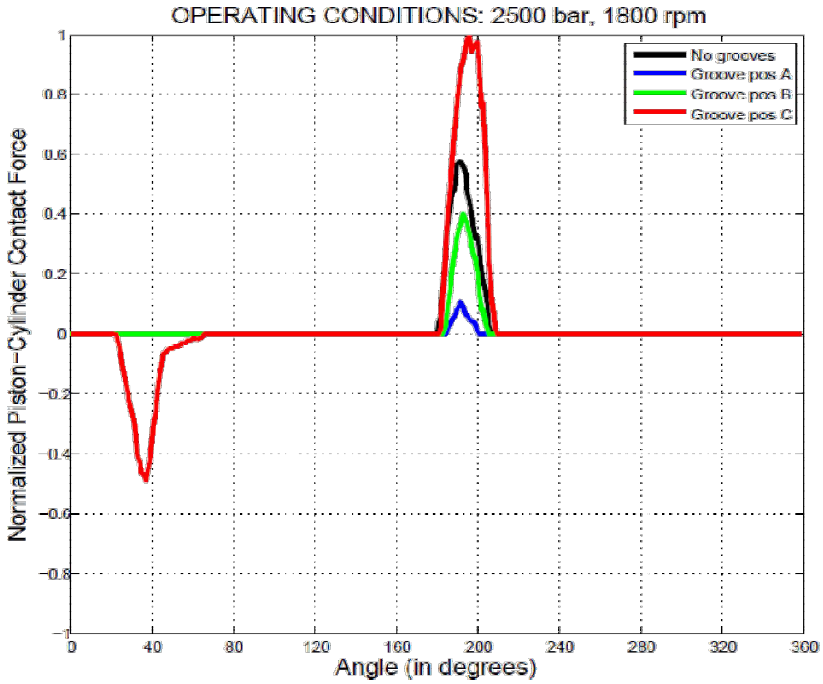

significantly reduced and the overall pump life can be improved.

Figure58:Regions of contact during a single pumping cycle at Pump outlet pressure is 2500 bar, and the shaft speed is 1800 rpm.

Another crucial point to remember is that the contact force increases with the distance between the groove and the piston's end that houses the displacement chamber. Because a full film lubrication assumption is made, the observed contact force trend might possibly lead to misleading conclusions in terms of pump performance, as shown in the next section. Groove Position 'A' has a better balance than the other examples (for both operating circumstances) because the hydrodynamic force created by the lubricant owing to the squeezing effect is adequate to balance the load causing the piston to tilt.

Figure 59 depicts the improvement in piston balance achieved by properly locating the groove.

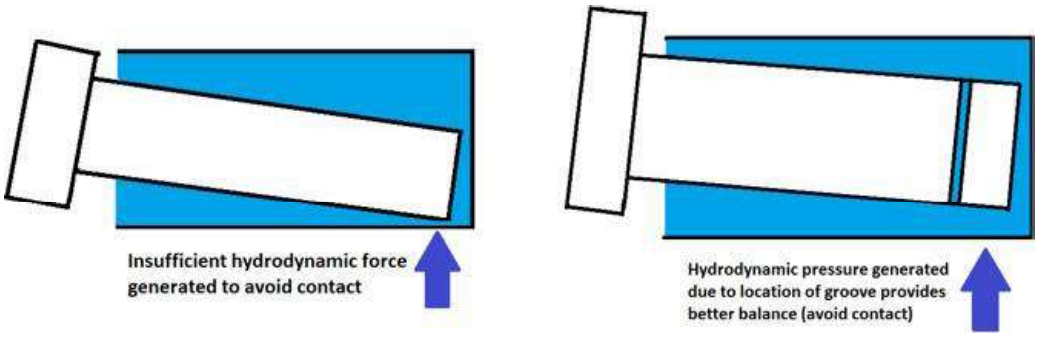

Figure 59: Illustration of the improvement in the piston balance due to additional hydrodynamic pressure generation enabled by the position of the groove on the piston.

At the same time, observing the effect of changing the position of the groove shows that a slight change in the position of the groove away from the end of the displacement chamber of the piston increases the expected metal-to-metal contact. By size and contact time. Therefore, it is important to optimize the groove position of each piston, especially when designing for long-term pump operation at ultra-high pressures under consideration. The important point to note here is that "optimal" groove positions, such as position "A", can reduce simulated metal-to-metal contact, but even in such cases there is an unavoidable contact force. You can see that there is. This gives confidence to the conclusion that mixed friction conditions may exist during a particular period of the pump cycle. Therefore, to design a radial piston pump with a long service life, it is necessary to test a modeling technique based on mixed lubrication. This will be discussed in more detail in the next chapter, based on the methodology proposed in Section 3.3 of Chapter 3.

5.2.3 Effect of Piston Grooves on the Lubricating Performance

The effect of a single groove on the balance of the piston was studied. Other configurations can be considered for pump performance analysis. Figure 60 shows the fluid network for all groove configurations considered in this section. Pump performance was analyzed under both operating conditions shown in Table 3.

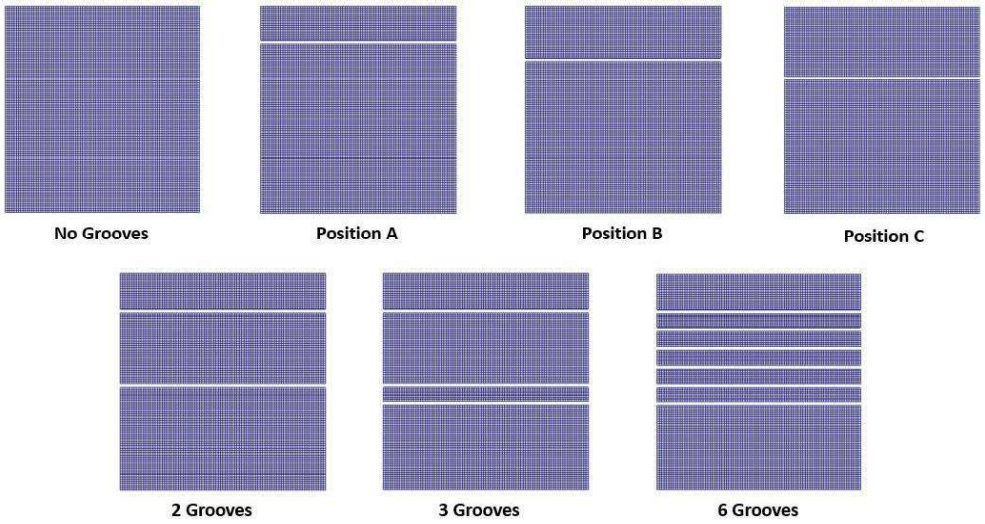

Figure 60: Computational grids were developed for the fluid regions of numerous pistons with various groove shapes.

Table4:Pump outlet pressure conditions Performance metrics recorded per shaft rotation in steady state: 700 bar, Shaft speed: 1800 rpm.

Piston Configuration	Power loss due to Leakage [% of total losses]	Power loss due to Viscous friction [% of total losses]	Volumetric Efficiency [%]
No Grooves	8.03	0.34	92.57
Position A	8.71	0.33	91.99
Position B	8.74	0.33	91.97
Position C	8.77	0.33	91.94
2 Grooves	8.22	0.34	92.41
3 Grooves	7.96	0.34	92.63
6 Grooves	7.45	0.37	93.07

Table5:Under steady-state conditions, efficiency metrics were measured per shaft revolution at 2500 bar pump outlet pressure and 1800 rpm shaft speed.

Piston Configuration	Power loss due to Leakage [% of total losses]	Power loss due to Viscous friction [% of total losses]	Volumetric Efficiency [%]
No Grooves	13.88	0.38	87.81
Position A	14.28	0.36	87.50
Position B	14.36	0.36	87.45
Position C	14.82	0.36	87.37
2 Grooves	12.95	0.37	88.53
3 Grooves	12.66	0.37	88.77
6 Grooves	12.07	0.38	89.23

FromTables4and5,there area few notable observations in the trend for the performance parameters of the pump:

• The location or number of grooves does not appear to play a major role in affecting viscous power loss at the piston / cylinder interface.

• With the introduction of single grooves, improved piston balance reduced piston-cylinder contact and increased leaks (decreased volumetric efficiency). However, this increase in leaks is acceptable, especially as a better balance is expected. This conclusion is verified by considering the surface features of the mixed friction model in Chapter 6.

• Increasing the number of grooves reduces power loss due to leaks (improves volumetric efficiency). This can be due to the fact that as the number of grooves located away from the edge of the displacement chamber increases, the piston becomes unbalanced and more contact is made to the piston / cylinder interface. This "contact" tends to better seal the interface (assuming full film lubrication conditions), but the larger the expected contact size, the more reliable the fact that a mixed lubrication regime may exist. Will increase. This can lead to inaccurate leak estimates for most notched piston designs that can be tested in simulation. Based on the comments above, optimization routines that can be tested to obtain the optimum groove parameters will give incorrect results based on the complete film assumptions. From this, it can be concluded that the study of the optimum circumferential groove design requires the evaluation of the mixed friction characteristics

CHAPTER 6

STUDYING THE IMPACT OF SURFACE ROUGHNESS AND SOLID ASPERITY USING THE MIXED FSI-EHD COUPLED MODEL PISTON BALANCE AND PUMP PERFORMANCE CONTACT

6.1 Significant Features of the Model

This chapter focuses on many aspects of the fully coupled mixed FSI-EHD model. As mentioned earlier, the main purpose of the design of this model was to investigate the effect of very low clearance (less than 2 m) on lubrication performance, especially under extreme operating conditions of ultra-high pressure. The lower the gap height, the more important the effect of the surface roughness of the solid body (piston and cylinder) becomes when simulating the flow at the piston-cylinder interface. As the importance of these surface imperfections grows, it becomes critical to mimic their elasto-plastic deformation when they interact appropriately. The genuine contact area between the bumps separates this occurrence from the nominal contact area supplied by the entire surface area of the undeformed bumps. As a result, the Lee and Ren (1994) model was used to quantify these impacts, and the observed contact areas at various time steps are shown in Figure 61. The comparable contact pressure created is also given. The data and comparisons shown here were obtained at an outlet pressure of 700 bar and a shaft speed of 1800 rpm. Figure 62 depicts the load support distribution based on the liquid film and contact area.As you can see, where the expected gap height is low, an increase in fluid pressure occurs as the fluid attempts to carry the load in those areas, and the bumps share part of the load. However, in areas of heavier asperity contact where the asperity contact pressure bears the majority of the load, the fluid pressure drops dramatically.

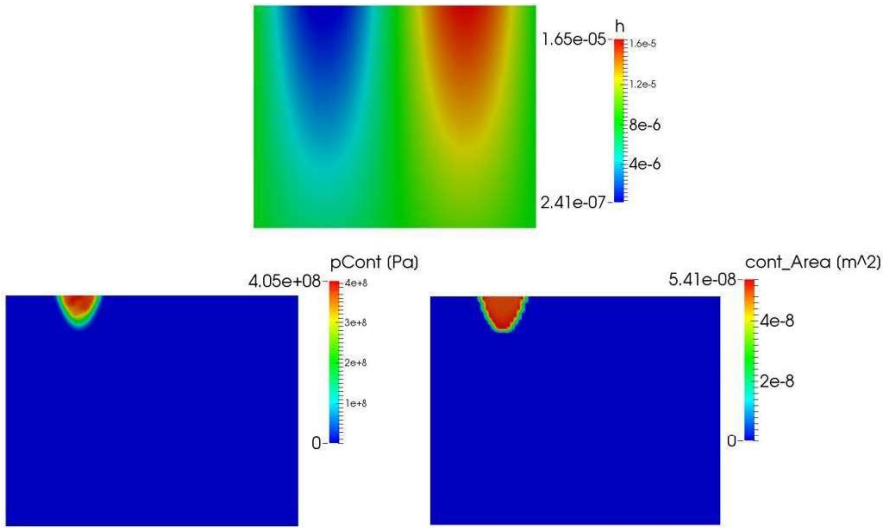

Figure61:Contact pressures and corresponding areas of contact were determined at low gap heights throughout the shaft rotation for Pump outlet pressure: 700 bar, Shaft speed: 1800 rpm.

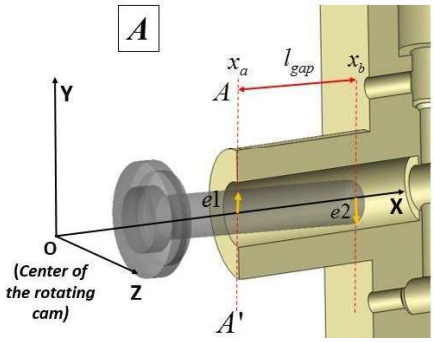

Figure62: Load support is shared between contact stresses and liquid pressures (red areas) and the breakdown of the liquid at extremely low gap heights (blue portions), when the load is mostly supplied by the contact stresses.

The combined lubrication effect may also be seen in the piston tilt scenario, as illustrated in Figure 63. The eccentricity of the pistons, denoted by e1 and e2, specifies the two sides of a quantity such as the piston separation distance. Low gap heights are occasionally observed as the piston eccentricities approach the order of the clearances between the cylinder and the cylinder. When a mixed lubricant is used, the piston tilt is lowered at certain points in the shaft rotation (180o 230o), as shown in the figure, when full film lubrication is expected.

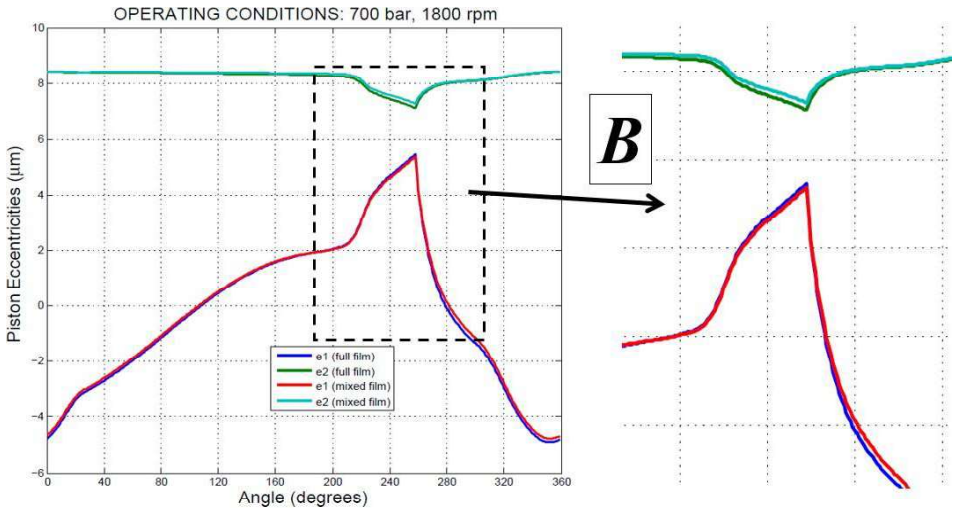

Figure 63: (A) Characteristics of piston tilt; (B) Comparison of piston tilt variation observed over one shaft rotation for complete film and mixed lubrication models. Pump outlet pressure: 700 bar, shaft speed: 1800 rpm.

The variation in specified minimum film thickness during the pump cycle is also influenced (Figure 64). When combined lubricating effects are taken into account, full film lubricating assumptions underestimate layer thickness during the exhaust stroke while overestimating it at the start of the distribution stroke. This can degrade pump efficiency by creating leak and viscous drag losses.

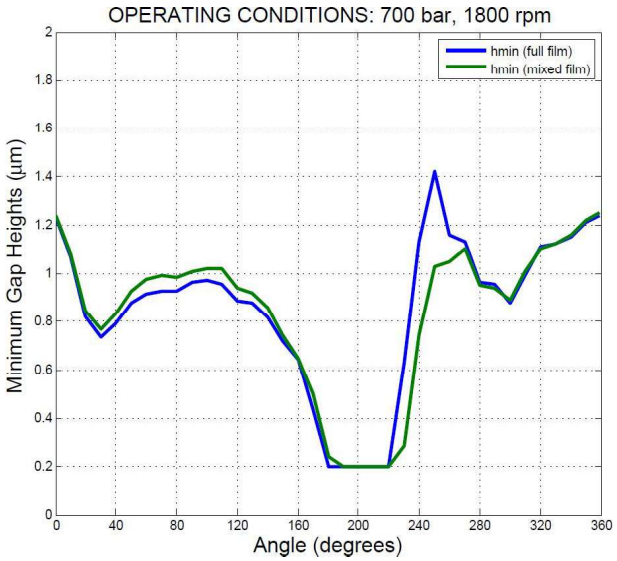

Figure 64: For the fluctuation of the minimum gap height above one shaft rotation, changes in trends were detected between full film and mix lubricating models for Pumps outlet pressure: 700 bar, Shaft speed: 1800 rpm.

This simulation may also be used to explore the effect of surface roughness on impact loads. The model may look into Gaussian surface roughness distributions, with the magnitude of the standard error rough variable Rq changing based on the manufacturing technique used to make the pistons and cylinders. Figure 65 depicts the change in contact load produced by axis angle for various degrees of surface roughness.

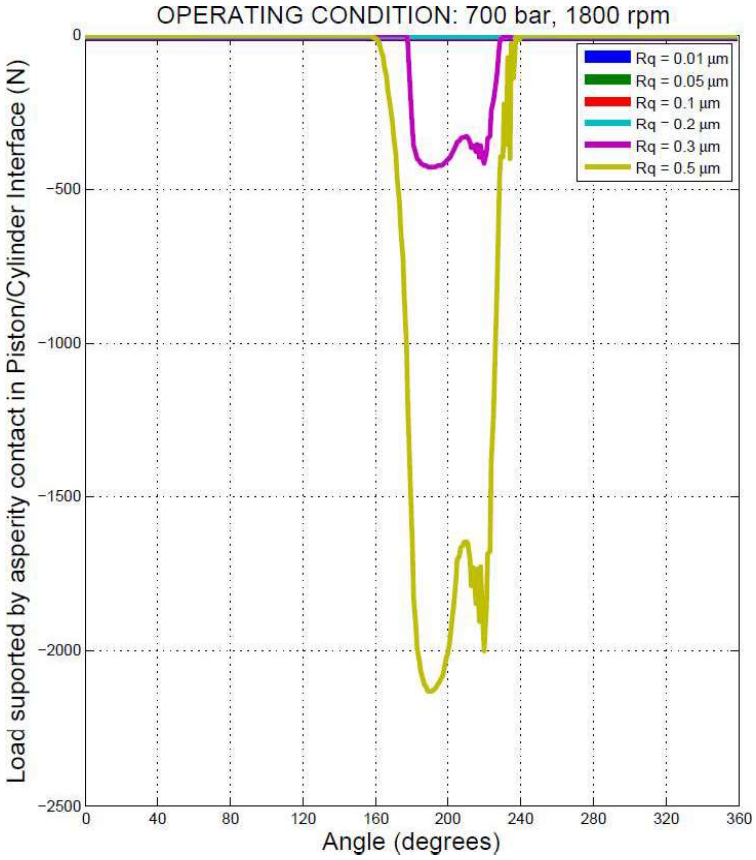

Figure 65: As a result, as the surface texture variable varies throughout a pumping cycle, the load borne by asperities changes. Pump outlet pressure is 700 bar, and the shaft speed is 1800 rpm.

It is clear that as surfaces get smoother, the fluid film becomes more stable (Rq 0.2m). Until Rq surpasses 0.3 m, surface roughness has little effect. As the asperities develop in size, the connections between them strengthen, allowing the asperities to sustain weights other than fluid. As a result, a smooth polished texture may be obtained, assisting in piston balancing and providing full film lubrication at the piston/cylinder contact.However, for the purposes of this experiment, a Rq = 0.5 m surface polish was chosen since it is the most commonly seen degree of finish, particularly in lubricated equipment. Similar surface quality has also been seen and repeated in bearing system studies (including conformal connections) [34, 35].

The combined FSI-EHD model was used to evaluate the impact on a single pump using the surface characteristics listed in Table 6.

Table6:Surfaces characteristics and variables that were employed in the simulations.

Surface Parameter	Description	Value [unit]
C	Piston/Cylinder Clearance	8 μm
R_q	Standard Deviation of the combined surface roughness	0.5 μm
R_{q1}	Average piston asperity height	0.03 μm
R_{q2}	Average cylinder asperity height	0.03 μm
Material	Piston and Cylinder materials	Steel
E_Y	Young's modulus of piston and cylinder	210 GPa
ν_1	Poisson's ratio of piston material	0.3 (-)
ν_1	Poisson's ratio of cylinder material	0.3 (-)

6.2 Prediction of Piston Balance

The four designs, namely 'No Groove,' Positions 'A,' 'Position B,' and Position 'C,' are contrasted in Figures 67 and 68 for the two dissimilar conditions indicated to demonstrate how the position of a circular groove effects piston balance. '

According to the contacting load trend, pumps with piston grooves closer to the displace chamber end (Position 'A') endure the least amount of force and hence have superior hydrodynamic balance. When the groove is pushed away from the end of the displaced chamber, the balance worsens.

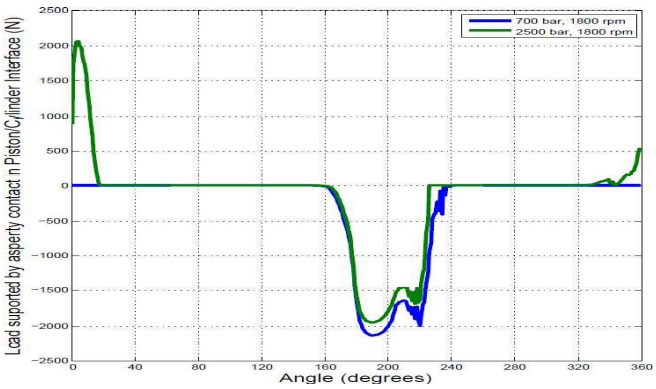

Figure66: Variation of load sustained by asperity contact in the piston/cylinder interface under two operating conditions: Pump outlet pressures vary from 700 to 2500 bar, with an 1800 rpm shaft speed.

The four designs, namely 'No Groove,' Positions 'A,' 'Position B,' and Position 'C,' are contrasted in Figures 67 and 68 for the two dissimilar conditions indicated to demonstrate how the position of a circular groove effects piston balance. '

According to the contacting load trend, pumps with piston grooves closer to the displace chamber end (Position 'A') endure the least amount of force and hence have superior hydrodynamic balance. When the groove is pushed away from the end of the displaced chamber

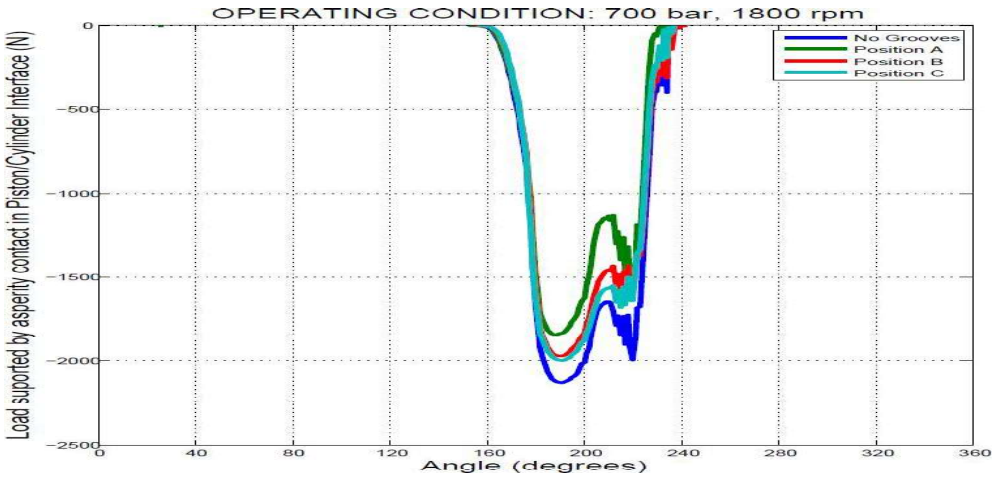

Figure67: The effect of cylinder groove location on impingement loads in the piston/cylinder contact at a pump discharge point of 700 bar and a shaft speed of 1800 rpm.

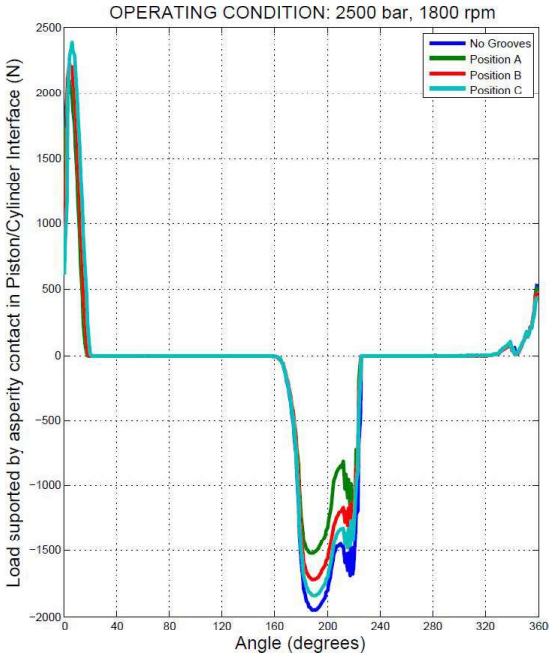

Figure 68: The effect of piston groove location on impingement contact strain in the piston/cylinder contact for pump output pressure: 2500 bar, shaft speed: 1800 rpm.

6.3 6.3 Prediction of Pump Performance

Tables7 and 8 show the predicted efficiency characteristics for the two operating circumstances using the four different piston designs that have been examined. Similar to what was found with the full film lubricating assumptions, the trend shows that leak losses increase as the grooves are moved farther away from the piston's displace chamber end, although viscous energy losses appear to be of the same size.

Table 7: Performance metrics measured per shaft revolution under steady-state circumstances at Pump outlet pressure: 700 bar, Shaft speed: 1800 rpm, and mixed lubrication.

Piston Configuration	Power loss due to Leakage [% of total losses]	Power loss due to Viscous friction [% of total losses]	Volumetric Efficiency [%]
No Grooves	8.72	0.32	91.98
Position A	8.74	0.33	91.96
Position B	8.75	0.33	91.96
Position C	8.78	0.32	91.93

Table8:During steady-state conditions, efficiency metrics per shaft rotation were measured at Pumps output pressure: 2500 bar, Shaft speed: 1800 rpm, and mixed lubrication.

Piston Configuration	Power loss due to Leakage [% of total losses]	Power loss due to Viscous friction [% of total losses]	Volumetric Efficiency [%]
No Grooves	14.11	0.36	87.64
Position A	14.25	0.36	87.53
Position B	14.28	0.36	87.51
Position C	14.31	0.36	87.49

Figures 69-71 show how employing mixed lubrication instead of complete film assumptions affects the efficiency metrics provided for every triple groove placement geometry when compared to a piston with no groove.

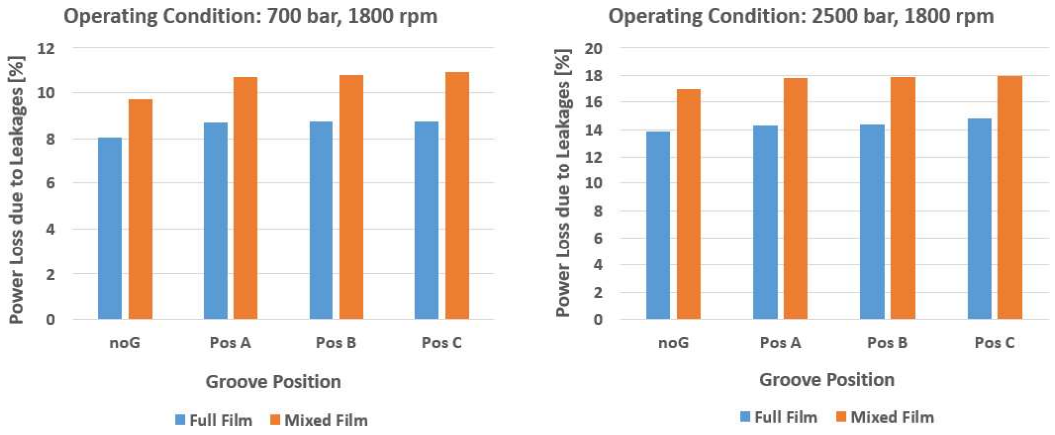

Figure 69: Using full film or mixed lubricant models, a percentage power loss owing to thick gooey friction was calculated for all four piston designs (left) The output pressure of the pump is 700 bar, and the shaft speed is 1800 rpm (right) The pump output pressure is 700 bar, and the shaft speed is 1800 rpm.

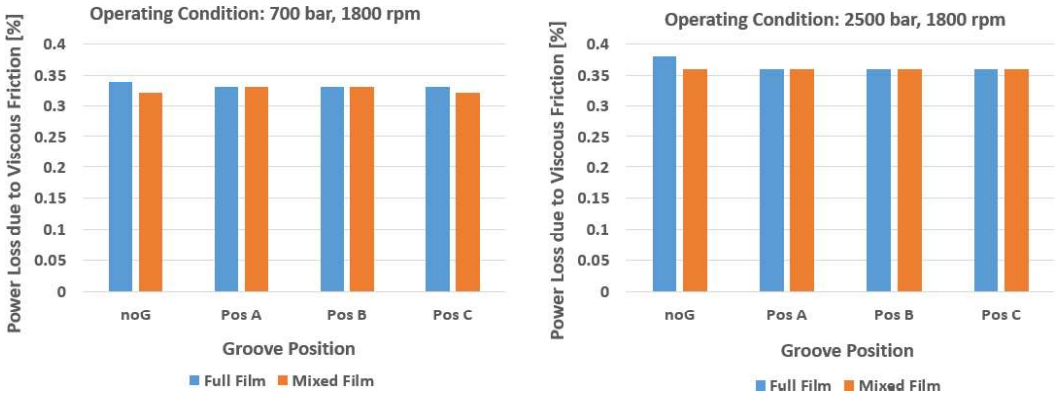

Figure70:Using full film or mixed lubricant models, a percentage power loss owing to thick gooey friction was calculated for all four piston designs (left) Pumping output pressure: 700 bar, shaft speed: 1800 rpm (right) Pump output pressure: 700 bar, shaft speed: 1800 rpm.

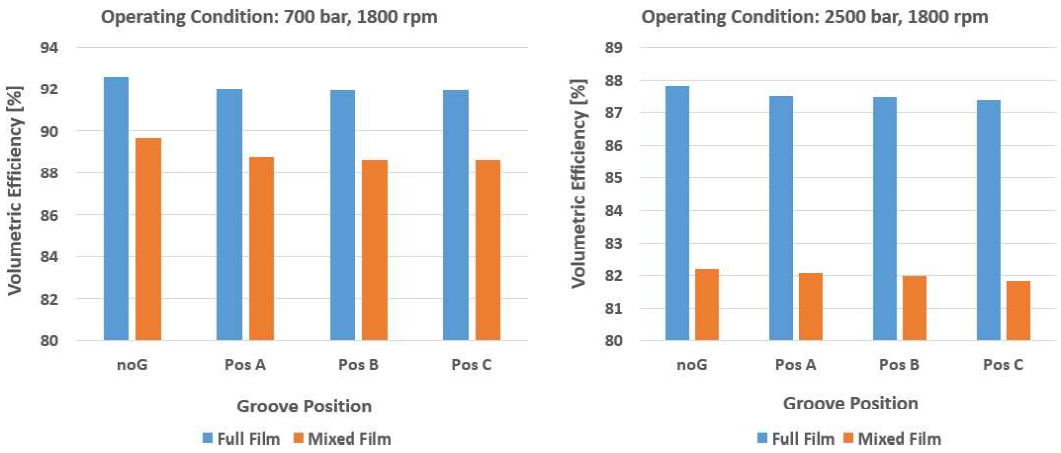

Figure 71: Volumetric Efficiency increases are correlated utilizing comprehensive film and mix lubricant simulations for all four piston designs (left) Pump pressure drop: 700 bar, left shaft speed: 1800 rpm, and (right) Pump outlet push: 700 bar, Propeller speed: 1800 rpm on the right.

A heterogeneous lubrication approach for the cam/piston contact, along with the addition of squeezing forces, may result in even better piston micro-motion predictions. Finally, an optimization process might be devised to assist in the development of the most effective and long-lasting groove piston design for various radial piston equipment and associated components.

The viscosity friction loss, on the other hand, is expected to be extremely close to that calculated using the whole film model. If thermal distortion of the surface and asperities caused by viscosity heat and heat exchange are incorporated, the viscous drag losses may be estimated more accurately. This is an area where the present model might be improved in the future.

CHAPTER 7

CONCLUSIONS

A fluid-structure-interaction-electro hydrodynamic model of piston / cylinder contact is offered, as well as a mix of empirical and framework approaches for evaluating bio dynamics and drag in cam / piston contact. I did. These two lubricating contacts are the primary source of energy loss in radial piston engines. These estimates of energy loss were made possible by developing a separate module to represent each interface while maintaining a close link between the two entities via data exchange. Using a previously generated global fluid flow model, describe the flow via the radial piston device to capture flow variations inside the piston / cylinder lubrication gap. A continuity equation was provided. The balance of force, which has a hemodynamic influence on the gap, can simulate the piston's tremor. The elastic deflection of the stiff body was measured by analyzing the liquid layer at an isothermal temperature (piston and cylinder). This allows the fluid in the lubrication contacts to withstand the load generated by the piston. That is, the contacts are completely lubricated.

The forces from the eccentricity cam and the instant created by the cam's force acting on the pistons were identified to be the two components influencing the piston's total micro-motion during the assessment of the piston's power balancing. Therefore, to improve the piston/cylinder spacing model's ability to predict the micro-motions of the pistons, a precise estimate of the change in the friction factor must be supplied as an input.As a result, a computer model was developed to predict viscous friction at the Cam/Piston interface, taking into account the impacts of hydrodynamic lubrication and non-Newtonian fluid behavior caused by the high sliding velocity between the cam and each piston's surface .However, the addition of rolling component bearings between the eccentric cam and an unconstrained outer race whose behavior is influenced by the dynamic of the four pistons makes calculating the frictional variance between the cam and each piston during a pumping cycle more challenging. An experimental setup was constructed in which the immediate rotational velocity of the raceway was found using a camcorder in order to provide exact inputs of the raceway's kinematic to the frictional model.

This method provides for a more precise computation of the coefficient of friction as a function of shaft angles, as well as a more precise prediction of energy loss owing to leakage and adhesive resistance at piston/cylinder contact. The friction model's further improvement has also resulted in the prediction of adhesive energy loss in cam / piston contact. Because of the related high slip speed, these losses were found to be larger than those recorded for piston/cylinder contact. It was discovered that a corrective force known as contact force was necessary to stabilize the piston in all of the scenarios and motion settings tested, as well as to assure the algorithm's numerical consistency. This requires the creation of unique methodologies for assessing the effects of surface quality and contact load ratio on machine lubrication efficiency.An EHD model based on the structural response of the mixed fluid was developed to take bumps into consideration as well as the effect of surface texture issues on the flowing fluid. The physical influence of wear orientation is mediated by coarse fat interactions, elasto-plastic delamination of abrasive particles caused by contact, and load balance between the fluid and the uneven surface. Everything is taken into account in this model. This enables better physics-based predictions of piston balance and lubrication efficiency, as well as a more precise understanding of groove effects. It was discovered that inserting a single groove at the end of the piston's displaced chamber offered the best piston balance in relation to the projected impact contact. Furthermore, the mixed lubrication method predicts pump performance with high variability, showing that the full film model overestimates leaks at piston / cylinder contacts. By developing this hybrid lubrication model, other novel aspects may be investigated. This study's findings reveal that numerical modelling of radial piston engines allows for virtual prototyping, which saves time, energy, and equipment as compared to manual development and testing. The effects of heat on both the lubrication gap and the model improvement process may be utilized to investigate gap flow. The use of non-uniform lubrication for cam / piston contact, as well as the incorporation of squish forces, can lead to more accurate forecasts of piston tremors. Finally, an optimization process can be developed to assist in the development of the most effective and durable grooved piston design for various radial piston appliances and the like.

LIST OF REFERENCES

1. Chapple, P. J. (1992). Modelling of a radial-piston hydraulic motor. Proceedingsof the Institution of Mechanical Engineers, Part I: Journal of Systems and ControlEngineering,206(3), 171-180.

2. Ivantysyn, J., & Ivantysynova, M. (2001). Hydrostatic pumps and motors. NewDelhi:AcademicBooksInternational.

3. Kleist,A. (1997).Designof Hydrostatic Static BearingandSealingGapsinHydraulicMachines.In 5thScandinavianInternationalConferenceonFluidPower, Linköping, Sweden, May(pp. 28-30).

4. Kleist, A. (1995). Berechnung von hydrostatischen Dichtstellen in hydraulischenMaschinen.Olhydraulik und Pneumatik, 39(10), 767.

5. Mortensen, K. A., & Henriksen, K. H. (2011). Efficiency Analysis of a RadialPiston Pump Applied in a 5MW Wind Turbine with Hydraulic Transmission.MasterThesis, AalborgUniversity, Aalborg, Denmark.

6. Agarwal, P. (2014). Modeling of High Pressure Radial Piston Pumps. MasterThesis,PurdueUniversity,Indiana, USA.

7. Fang,Y.,&Shirakashi,M.(1995).MixedLubricationCharacteristicsbetweenthe Piston and Cylinder in Hydraulic Piston Pump-Motor. Trans. ASME, JournalofTribology, 117.

8. Olems,L.(2000).Investigationsofthetemperaturebehaviourofthepistoncylinder assembly in axial piston pumps. International Journal of Fluid Power,1(1),27-39.

9. Wieczorek,U.,&Ivantysynova,M.(2002).Computeraidedoptimizationofbearingandsealing gapsinhydrostaticmachines—thesimulationtoolCASPAR. International Journal of FluidPower,3(1), 7-20.

10. Dhar, S.(2014). A Study of Fluid Structure and ThermalInteractionsin theLubricatingInterfaceBetweenGearsandLateralBushesinExternalGearMachines,Ph.D. Thesis,PurdueUniversity,Indiana, USA.

11. Pelosi, M., & Ivantysynova, M. (2010). A fully coupled thermo-elastic model forthe rotating kit of axial piston machines. In ASME/Bath Symposium on FluidPowerand Motion Control, Bath, UK, Sept(pp.15-17).

12. Pelosi,M.,&Ivantysynova,M.(2011).SurfaceDeformationsEnableHighPressure Operation of Axial Piston Pumps. In ASME 2011 Dynamic Systems andControl Conference and Bath/ASME Symposium on Fluid Power and MotionControl(pp. 193-200).American Societyof Mechanical Engineers.

13. Pelosi, M., & Ivantysynova, M. (2013). The Impact of Axial Piston MachinesMechanicalPartsConstraintConditionsontheThermo-

ElastohydrodynamicLubrication Analysis of the Fluid Film Interfaces. International Journal of FluidPower,14(3), 35-51.

14. Pelosi, M., & Ivantysynova, M. (2012). A geometric multigrid solver for thepiston–cylinder interface of axial piston machines. Tribology Transactions, 55(2),163-174.

15. Huang, C., & Ivantysynova, M. (2006). An advanced gap flow model consideringpiston micro motion and elastohydrodynamic effect. FPNI Ph.D. Symposium onFluidPower.

16. Pelosi,M.(2012).AnInvestigationontheFluid-StructureInteractionofPiston/Cylinder Interface,Ph.D.Thesis,PurdueUniversity,Indiana,USA.

17. Schenk,A.,&Ivantysynova,M.(2012).Theinfluenceofswashplateelastohydrodynamic deformation in the slipper-swashplate interface. FPNI Ph.D.SymposiumonFluid Power.

18. Schenk, A., Zecchi, M., & Ivantysynova, M. (2013). Accurate Prediction of AxialPistonMachine'sPerformancethroughaThermo-ElastohydrodynamicSimulation Model. ASME/Bath Symposium on Fluid Power and Motion Control.Sarasota,FL.

19. Zecchi, M. (2013). A Novel Fluid Structure Interaction and Thermal Model toPredict the Cylinder Block/Valve PlateInterface Performance in Swash PlateType AxialPistonMachines,Ph.D.Thesis,PurdueUniversity,Indiana,USA.

20. Zecchi, M., & Ivantysynova, M. (2012). An investigation of the impact of microsurface shaping on the cylinder block/valve plate interface performance through anovelthermal-elastohydrodynamicmodel,FPNIPh.D.SymposiumonFluidPower.

21. Zecchi, M., & Ivantysynova, M. (2012). Cylinder Block/Valve Plate Interface – ANovel Approach to Predict Thermal Surface Loads. International Fluid PowerConference(IFK).

22. Dhar S., & Vacca A. (2013). A Fluid Structure Interaction-EHD Model of theLubricatingGapsinExternalGearMachines:FormulationandValidation.TribologyInterna tional62:78-90.

23. Wang, Q. J., Shi, F., & Lee, S. C. (1997). A mixed-lubrication study of journalbearingconformal contacts. Journal ofTribology,119(3), 456-461.

24. Oh, K. P., & Goenka, P. K. (1985). The elastohydrodynamic solution of journalbearingsunder dynamicloading. Journal ofTribology,107(3), 389-394.

25. Xiong, S., Lin, C., Wang, Y., Liu, W. K., & Wang, Q. J. (2010). An efficientelastic displacement analysis procedure for simulating transient conformal-contactelastohydrodynamiclubricationsystems.JournalofTribology,132(2),021502.

26. Stefani, F. A., & Rebora, A. U. (2002). Finite element analysis of dynamicallyloadedjournalbearings:influenceoftheboltpreload.JournalofTribology,124(3), 486-493.

27. Piffeteau, S., Souchet, D., & Bonneau, D. (2000). Influence of thermal and elasticdeformationsonconnecting-rodbigendbearinglubricationunderdynamicloading.Journalof Tribology, 122(1), 181-191.

28. Wu, S., & Cheng, H. S. (1991). A friction model of partial-EHL contacts and

itsapplicationto powerlossin spurgears. TribologyTransactions,34(3), 398-407.

29. Patir, N., & Cheng, H. S. (1978). An Average Flow Model for Determine Effectsof Three Dimensional Roughness on Partial Hydrodynamic Lubrication, ASMEJournalofLubrication Technology, Vol.100, pp.12-17.

30. Lee, S. C., & Ren, N. (1996). Behavior of Elastic-Plastic Rough Surface Contactsas Affected by the Surface Topography, Load and Materials, STLE TribologyTransactions, Vol. 39, pp. 67-74.

31. Meng, F, Wang, Q. J., Hua, D., & Liu, S. (2010). A Simple Method to CalculateContact Factor Used in Average Flow Model, ASME Journal of Tribology, Vol.132,pp. 024505-1 – 024505-4.

32. Chengwei, W., & Linqing, Z. (1989). An Average Reynolds Equation for PartialFilm LubricationwithaContactFactor,ASMEJournalofTribology,Vol. 111,pp.188-191.

33. Harp, S. R., & Salant, R. F. (2000). An average flow model of rough surfacelubrication with inter-asperity cavitation, ASME Journal of Tribology 123, pp.134–143.

34. Shi,F.,&Wang,Q.(1998).AMixed-TEHDStudyforJournal-BearingConformalContacts,PartI:ModelFormulationandApproximationofHeatTransfer Considering Asperity Contacts, ASME Journal of Tribology 120, pp.198-205.

35. Wang, Q. J., Shi, F., & Lee, S. C. (1997). A Mixed-TEHD Study for Journal-Bearing Conformal Contacts – Part II: Contact, Film Thickness, and PerformanceAnalyses,Journal of Tribology, pp. 206-213.

36. de Kraker, A., van Ostayen, R. A. J., & Rixen, D. J. (2007). Calculation ofStribeck curves for (water) lubricated journal bearings, Tribology International40(3),pp. 459-469.

37. Yamaguchi, A., & Matsuoka, H. (1992). A mixed lubrication model applicable tobearing/sealpartsofhydraulicequipment,Journaloftribology,114(1), 116-121.

38. Kazama, T., & Yamaguchi, A. (1993). Application of a mixed lubrication modelforhydrostaticthrustbearingsofhydraulicequipment. JournalofTribology115(4),686-691.

39. Kazama, T. (2005). Numerical simulation of a slipper model for water hydraulicpumps/motorsinmixedlubrication.In ProceedingsoftheJFPSInternationalSymposiumonFluid Power, Vol. 6,pp. 509-514.

40. Wegner, S., Loschner, F., Gels, S., & Murrenhoff, H. (2016) Validation of thephysical effect implementation in a simulation model for the cylinder block/valveplate contact supported by experimental investigations, Proceedings of the 10th InternationalFluid Power Conference, pp. 269-282.

41. Lasaar,R.(2003).EineUntersuchungzurmikro-undmakrogeometrischenGestaltung der Kolben-/Zylinderbaugruppe von Schraegscheibenmaschinen, VDIVerlagGmbH,Duesseldorf.

42. Hargreaves,D.J.(1991).Surfacewavinesseffectsontheload-carryingcapacityofrectangularslider bearings, Wear145, pp. 137-151.

43. Ivantysynova,M.,Garret,R.A.,&Frederickson,A.A.(2012).Positivedisplacement machine piston with wavysurfaceform, US 20120079936 A1.

44. Park, T. (2008). Lubrication analysis between piston and cylinder in high pressurepistonpumpconsideringcircumferentialgroovesandviscosityvariationwithpressure, Proceedingsofthe9thBiennialASMEConferenceonEngineeringSystemsDesign and Analysis, Haifa,Israel.

45. Berthold,H.(1999).Axialpistonmachinehavingacoolingcircuitforthecylindersand pistons, US 5971717 A.

46. Majumdar, B. C., Pai, R., & Hargreaves, D. (2004). Analysis of water-lubricatedjournalbearingswithmultipleaxialgrooves,Availablefrom: <http://pij.sagepub.com/content/218/2/135.full.pdf>.[25April2015].

47. Basu,P.(1992).Analysisofaradialgroovegasfaceseal.STLETribologyTransactions 35(1):11–20.

48. Razzaque,M.M.,&Kato,T.(1999).Effectsofgrooveorientationonhydrodynamicbehaviorof wetclutchcoolantfilms,TransactionsofASME121:6–61.

49. Kumar, S., Bergada, J. M., & Watton, J. (2009). Axial piston pump groovedslipperanalysisbyCFDsimulationofthreedimensionalNVSequationincylindricalco ordinates,ComputationalFluids38:648–63.

50. Kumar, S., & Bergada, J. M. (2009). The effect of piston grooves performance inan axial piston pumps via CFD analysis,International Journal of MechanicalSciences66:168-179.

51. Agarwal, P., Vacca, A., Kim K., and Kim, T. (2014) A numerical model for thesimulation of flow in radial piston machines, Proceedings of the InternationalExpositionforFluid Power,Las Vegas,USA.

52. Agarwal,P.,Vacca,A.,Wang,K.,Kim,K.etal.(2014).AnAnalysisofLubricating Gap Flow in Radial Piston Machines, SAE International Journal ofCommercialVehicles7(2): 524 – 534.

53. Vacca,A.,&Guidetti,M.(2011).Modellingandexperimentalvalidationofexternal spur gear machines for fluid power applications. Simulation ModellingPracticeandTheory, 19(9), 2007-2031.

54. OpenFOAM: The Open Source CFD toolbox. Available at: www.openfoam.com.Accessed July7, 2016.

55. GNUScientificLibrary.Availableat:http://www.gnu.org/software/gsl/.AccessedJuly7, 2016.

56. ANSYS, Inc.Available at:http://www.ansys.com/.AccessedJuly7,2016.

57. Reynolds, O. (1886). On the Theory of Lubrication and Its Application to Mr.Beauchamp Tower's Experiments,Including an Experimental Determination ofthe Viscosity of Olive Oil. Proceedings of the Royal Society of London, 40(242-245),191-203.

58. Jasak, H., & Weller, H. G. (2000). Application of the finite volume method andunstructuredmeshestolinearelasticity.Internationaljournalfornumericalmethodsin engineering,48(2), 267-287.

59. Booser,E.R.(1983)CRChandbookoflubrication(theoryandpracticeoftribology)– Volume 1.Application and maintenance, CRCPress.

60. Hamrock, B. J., Schmid, S. R., and Jacobson, B. O. (2004). Fundamentals of fluidfilmlubrication, 2 ed. CRC press.

61. Dowson, D., and Higginson, G. R. (1966). Elasto-hydrodynamic lubrication: thefundamentalsofroller andgear lubrication,2 ed.,Oxford:Pergamon Press.

62. Barus, C. (1893).Isothermals, isopiestics and isometrics relative to viscosity,AmericanJournal of Science 266: 87 -96.

63. Jacobson,B.O.,andHamrock,B.J.(1984).Non-Newtonianfluidmodelincorporated into elastohydrodynamic lubrication of rectangular contacts. Journalof Tribology106(2): 275-282.

64. Wang,J.,Venner,C.H.,andLubrecht,A.A.(2013).InfluenceofSurfaceWavinessontheTherma lElastohydrodynamicLubricationofanEccentric-Tappet Pair. Journal of Tribology135(2): 021101-1 -021101-12.

65. Patir,N.,&Cheng,H.S.(1979).ApplicationofAverageFlowModeltoLubrication Between Rough Surfaces, ASME Journal of Lubrication Technology,Vol.101, pp. 220-22

International Journal of All Research Education & Scientific Methods

UGC Certified Peer-Reviewed Refereed Multi-disciplinary Journal
ISSN: 2455-6211, New Delhi, India
Impact Factor: 7.429, SJR: 2.28, UGC Journal No. : 7647

Acceptance Letter

Dated: 22/06/2022

Dear Authors,

We are glad to inform you that your paper has been accepted as per our fast peer review process:

Authors Name: **Mr yaqoob Ali Ansari**

Paper Title: **Modeling The Lubricating Interfaces Of Ultra-High Pressure Radial Piston**

Paper Status: **Accepted**

Paper Id: **IJ-2206221133**

for possible publication in **International Journal of All Research Education & Scientific Methods, (IJARESM), ISSN No: 2455-6211", Impact Factor : 7.429**,

in the current Issue, **Volume 10, Issue 6, June - 2022**.

Kindly send us the payment receipt and filled copyright form asap. Your paper will be published soon after your payment confirmation.

Best Regards,

Editor-in-Chief,
IJARESM Publication, India
An ISO & UGC Certified Journal
http://www.ijaresm.com

MODELING THE LUBRICATING INTERFACES OF HIGH PRESSURE RADIAL

by National Printers

Submission date: 04-Jul-2022 12:29PM (UTC-0400)
Submission ID: 1849701912
File name: NG_THE_LUBRICATING_INTERFACES_OF_HIGH_PRESSURE_RADIAL.docx (4.73M)
Word count: 18428
Character count: 99169

ORIGINALITY REPORT

19%	19%	1%	0%
SIMILARITY INDEX	INTERNET SOURCES	PUBLICATIONS	STUDENT PAPERS

MATCH ALL SOURCES (ONLY SELECTED SOURCE PRINTED)

Internet Source

Exclude quotes	On	Exclude matches	< 10%
Exclude bibliography	On		